# Multiple Feed Reflector Antenna Analysis

by

Scot Howard Stewart

Thesis submitted to the Faculty of the

Virginia Polytechnic Institute and State University

in partial fulfillment of the requirements for the degree of

Master of Science

in

Electrical Engineering

APPROVED:

W. L. Stutzman, Chairman

R. C. Robertson

T. Pratt

June 1986

Blacksburg, Virginia

# Multiple Feed Reflector Antenna Analysis

by

Scot Howard Stewart

W. L. Stutzman, Chairman

Electrical Engineering

(ABSTRACT)

A method of calculating the secondary pattern of a reflector illuminated by a feed array is developed. Geometrical optics is used to determine the incident field via a coordinate transformation approach. The incident field from each element is superimposed to form the total field used in finding the surface currents of the physical optics radiation integral. The technique allows each element to be arbitrarily excited, positioned and oriented. The element patterns may be different allowing mutual coupling to be included.

## ACKNOWLEDGEMENTS

I would like to thank my family (especially Martha) for their support during the good and bad of this endeavor. My thanks to the Stutzmans who constantly brought laughter into my life and to Wendy who "bore" with me through the typing. Finally, to my advisors and those "unsung heros" (especially M. Sockell) who were patient enough to listen and then offer ideas and suggestions to this material.

TABLE OF CONTENTS

## TABLE OF FIGURES

## LIST OF TABLES

# 1. INTRODUCTION

Reflector antennas are widely used when high gain is needed, such as in communications and radar applications. The gain of a reflector antenna can be approximated using rule-of-thumb techniques that only require an estimate of the aperture efficiency. These techniques are soon abandoned when complicated geometries and high accuracies are needed. Many techniques exist for accurate computation of the secondary pattern of reflector antennas. The most widely used methods are discussed in Chapter 2.

An approach is suggested here based on physical optics (P.O.) concepts that are capable of accurately predicting main beam, near-in side lobes and cross polarization properties. The technique is detailed in Chapter 3 where theoretical formulations and algorithms are presented. The method was programmed and given the acronym RAP (Reflector Analysis Program). The full documentation of RAP is presented in [1]; however, important aspects are repeated for completeness. The program has since been expanded to allow multiple feed element reflector geometries to be analyzed.

Multiple feed reflectors are of considerable interest especially for the design of satellite antennas for either contoured or spot beam applications. These beam types require simultaneous or subsidiary

excitation of multiple element feed arrays. The technique presented here allows any practical feed array to be analyzed. The method employs superposition of the element radiation patterns onto the reflector surface. Most multi-element feed analysis techniques apply superposition to the secondary (reflected) far-field patterns. However, the near-field approach presented here is superior in three areas:

(i) Accurate feed array spillover values can be obtained leading to accurate gain and efficiency values.

(ii) The multi-element feed can be analyzed almost as fast as a single element and requires far less file management.

(iii) The elements can be arbitrarily located and pointed which is ideal for feed location and pointing optimization studies.

Chapter 4 presents the multiple feed element analysis technique. The method is based largely on the approach given in Chapter 3. The accuracy of the method has proved to be excellent.

The multiple feed element analysis technique was programmed and given the acronym MFRAP (Multiple Feed Reflector Antenna Program). The coding approach builds on that of RAP; therefore, only the differences between the codes are discussed here. Chapter 5 gives an overview of MFRAP along with discussions simplifying the complicated geometries encountered in a multiple feed system. The input file formats and code accuracy are discussed.

# 2. REFLECTOR ANALYSIS TECHNIQUES

Many approaches have been developed to analyze electrically large (diameter > 10λ) reflector antennas. The common techniques are summarized in Table 2.0 [2]. First these techniques are briefly outlined. Then in following sections the most popular of these methods are discussed in greater detail, namely geometrical optics (GO), physical optics (PO) and the geometrical theory of diffraction (GTD).

Table 2.0

**Reflector Antenna Analysis Approaches**

- Ray Tracing
- Asymptotic Methods
- GTD (Geometrical Theory of Diffraction)
- Radiation Integral Methods
  - Analytic integration
  - Direct numerical integration
  - Series representation
  - Sampling methods

Ray Tracing (also called geometrical optics) is used mainly for shaped radiation pattern analysis and is not applied to high accuracy situations such as high gain, low side lobe patterns that are of concern to us.

Asymptotic methods are closely related to conventional ray tracing techniques and have been applied to high gain reflector antennas. [3]

GTD methods are very useful in reflector analysis but cannot be used alone. The GTD solution can "blow up" along shadow boundaries and caustics (on-axis). [4] The GTD method is used in combination with a radiation integral method (used to find near-axis fields). In fact, GTD methods are usually used to find radiated fields (due to edge diffraction) beyond the shadow boundaries where conventional radiation integral methods become inaccurate. The GTD based aperture field method usually ignores the axial component of the equivalent surface current leading to inaccurate cross polarization calculations. [3] The GTD method is detailed in Section 2.2.

Radiation integral methods use current or aperture field approaches. The relative merits of these are discussed later in Section 2.1. Both involve evaluation of a radiation integral.

## 2.1 GEOMETRICAL OPTICS/PHYSICAL OPTICS

Without a doubt the most common analysis approaches are by geometrical or physical optics techniques. These methods are similar in that they both involve the generation and evaluation of the radiation integral. They are popular because they can be used to accurately predict the main beam and close in side lobes; furthermore, they can be used with GTD to increase the far-out sidelobe accuracy and computational efficiency.

Even though there are similarities between the two methods, there are also important differences. It is then necessary to choose between the two approaches. Note however that there is less than unanimous agreement among researchers in the field as to whether the additional complexity of the physical optics approach is warranted. In this section we will present some of the major conclusions reported in the literature.

For parabolic shaped reflectors the solutions (G.O. and P.O.) yield identical results at boresight. [5] Rudge et al. [8, p.77] state that in directions far from the reflector axis the G.O. formulation introduces a significant path-length discrepancy. Rusch and Potter [6, p.52] attribute the superior accuracy of the surface current formulation to its inclusion of axially directed reflector currents that are not present in the G.O./aperture field method.

On the other hand, Rudge [7, 8] claims there is no clear answer to which formulation in inherently more accurate and suspects the effects

of truncation of the equivalent currents in the physical optics approximation may mask other differences. He examined systems of equivalent electric current, equivalent magnetic current, or both on the reflector surface and on the aperture plane.

Rahmat-Samii [9] examined pattern calculations of the techniques for offset reflectors. He showed that the G.O./aperture integral method gives a symmetric pattern even in the offset plane. However, the P.O./surface integral method gives asymmetric results for offset reflectors (even with symmetric feed patterns). He notes that if the diffracted rays (GTD) are included in the aperture field with the G.O. contribution, the phase of the integral is no longer constant (because of different optical paths of edge diffracted rays); an asymmetric pattern can then result in the plane of offset. Rahmat-Samii compared measured data from Rudge [10] for an offset parabolic reflector (diameter = 28.6$\lambda$) to his calculations with the P.O./surface current method. Asymmetries in side lobe heights and null locations in the copolarized pattern and crosspolar peaks were reproduced well with the calculations. In this particular case, deviations of the G.O./aperture field method were not major and thus the increased accuracy of the P.O./surface current method was not dramatic.

Hasselmann and Felsen [3] referenced the work of Adatia [11] in claiming that the cross polarization predicted by P.O. may be of the same order as errors in the specification of the surface currents. This appears to contradict the excellent agreement just noted above in the work of Rahmat-Samii [10].

As a final note Kildal [5] used GTD analysis to evaluate the accuracy of gain calculations based on P.O. He presented the following upper bound

$$\Delta G \simeq 0.22\ (\lambda/D)^2 \quad dB$$

## 2.2 GEOMETRICAL THEORY OF DIFFRACTION - GTD

Over the last two decades many papers have presented GTD approaches to solving the reflector antenna radiation problem. The technique is accurate, efficient and simple to use. It however cannot be used alone for it has singularities at shadow boundaries and caustics (on-axis). Therefore, G.O. or P.O. techniques are often augemented by GTD combining to form both accurate and efficient analysis of reflector antennas.

GTD is a popular technique for it is highly efficient, often orders of magnitude faster than comparable P.O. techniques for large structures [12]. Instead of evaluating the large and complicated P.O. radiation integral, GTD represents individual reflected or diffracted rays which geometrically satisfy the generalized Fermat's principle. [13] The increased accuracy of the GTD technique over the P.O. method is seen from the asymptotic series expansion of the far-field. [12] It is shown that P.O. gives an approximate solution which is asymptotically correct only on the order of $k^0$ ($k = 2\pi/\lambda$). On the other hand, using GTD with the

uniform asymptotic theory of diffraction yields scattered fields accurate to the $k^{-1/2}$ order [12].

Whether G.O. or P.O. are used alone or in conjucntion with GTD techniques the radiation integral must be generated and evaluated. The additional complexity of adding GTD is hardly warranted in many cases. The size of reflectors considered here ($10\lambda \leq D \leq 100\lambda$) do not present computer run time problems. In any event, the suggested technique developed in the next section can be expanded to include GTD analysis.

## 2.3 A SUGGESTED APPROACH

The selection of an analysis approach (see Table 2.0) depends on the specific application. Here we are concerned with gain (aperture efficiency) and near-in side lobes of moderately sized reflector antennas. For this application the radiation integral methods are the clear choice because they yield the main beam and first several side lobes: these in turn primarily influence the gain. It is also logical to choose the physical optics/surface current formulation because of its reported higher accuracy. It is only slightly more difficult than the G.O./aperture field method since the integration over the reflector surface can be replaced by an integration over a projected area on the aperture plane. This is detailed later in this section.

The choice of how to evaluate the radiation integral is clear. For reflectors that are not extremely large (greater than about 50 or 100λ) direct numerical integration can be applied without excessive computer run times. The only viable alternative is to employ expansion representations of the integral. The reported methods do offer improved computer run times for large reflectors, however, there are several drawbacks to such methods including the following: (a) Accuracy can be inferior especially for reflectors that are not large, (b) They can introduce significant formulation complexities which increase the opportunity for coding errors, and (c) There are severe restrictions on antenna geometry; such restrictions vary from mild, such as a circular projected aperture, to sever, such as an axisymmetric parabolic reflector.

The determining factor appears to be electrical size. In other words unless large reflectors are to be encountered direct numerical integration is preferred. Since we do not have that requirement the suggested approach is the physical optics/surface current formulation of the radiation integral method employing direct numerical integration. ..

The Reflector Antenna Program (RAP) was written using the approach suggested above. The method was taken from a paper by Y. R. Samii (et al.) because of its straightforward analysis and expansionary capabilities. [14]. S. W. Lee (et al.) has the extended the capability to include GTD from subreflectors of any shape [12]. The mathematical derivation is discussed next.

## 2.3.1 RADIATION INTEGRAL DERIVATION

The following derivation is based on the geometry given in Figure 2.3-1 where it is shown that the basic reflector antenna problem consists of three parts, each represented by its own coordinate system: 1) the feed (super 0), 2) the reflector/aperture (primed), and 3) the far field (unprimed). Generally the radiation pattern of the feed is known (or assumed) in its own coordinate system. A transformation between feed and reflector (a geometrical optics approach) is used to determine the reflector illumination. The surface currents ($\vec{J}$) formed are functions of feed illumination, reflector position and reflector orientation. The currents are summed to produce a far-field radiation pattern. The summation is performed by a radiation integral; the full derivation can be found in [1]. The physical optics radiation integral is presented next.

The electric field intensity in the far-field of a reflector with surface current density $\vec{J}$ on the lit portion of the reflector [1] is given as

$$\vec{E} = -jk\eta \frac{e^{-jkr}}{4\pi r} \int\int_{S_r} [\vec{J} - (\vec{J} \cdot \hat{r})\hat{r}] e^{jk\bar{r}'} \cdot \hat{r}_{ds'} \qquad (2.3.1\text{-}1)$$

where

$$\vec{J}(\bar{r}') = 2\,\hat{n} \times \vec{H}_c'$$

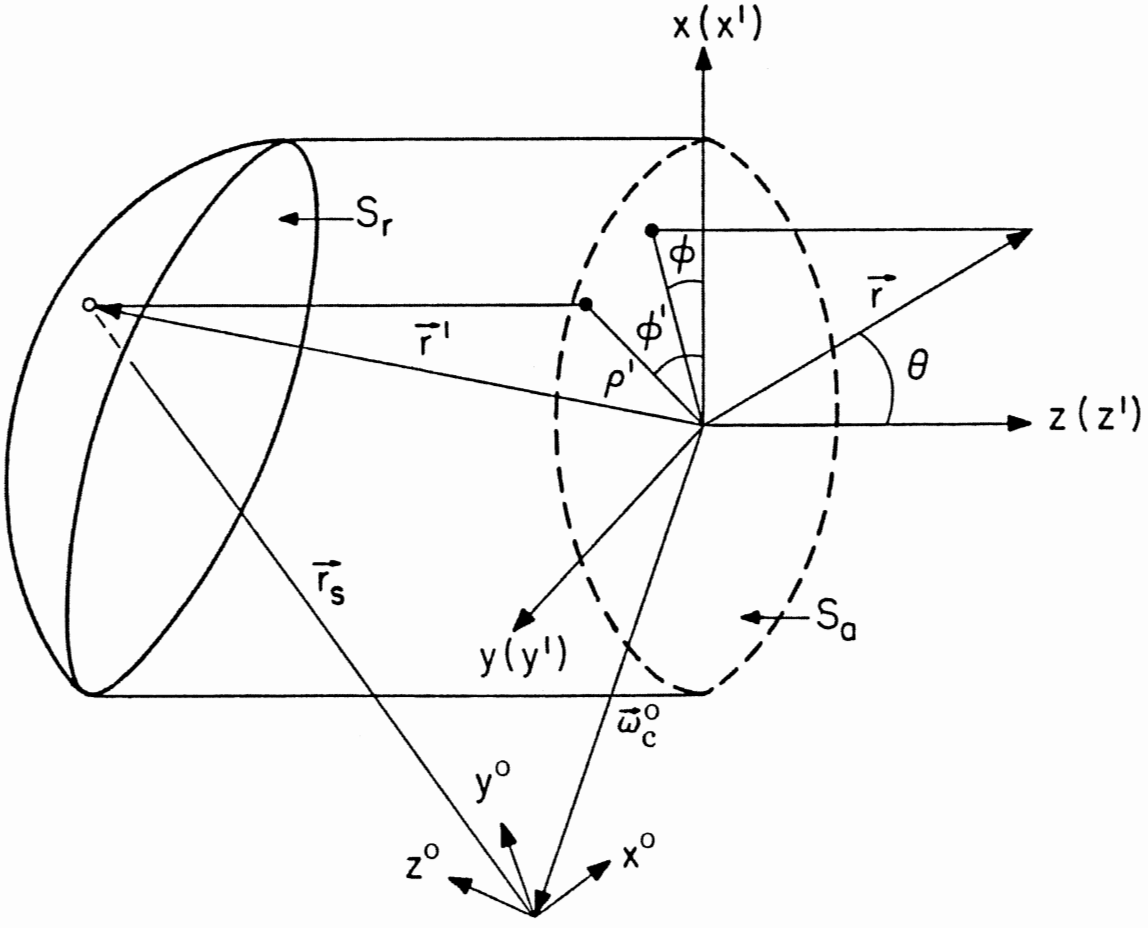


Figure 2.3-1 Reflector system geometry.

$\hat{n}$ = unit normal at reflector surface
gives orientation information,

$\vec{H}_c'$ = incident H-field relative to reflector coordinates
(prime) consisting of Cartesian components
(subscript c) gives intensity information,

$\bar{r}'$ = position vector where $\hat{n}$ and $\vec{H}_c'$ are defined
relative to the reflector system (primed) gives
location information.

The implicit assumptions in the result are:

1. The physical optics approximation, where the fields from the feed evaluated at the illuminated portion of the reflector are used to find the current excited there and currents are zero elsewhere.

2. An electric current exists.

3. The reflector is large relative to a wavelength.

4. Radii of curvature of the reflector are large relative to a wavelength.

5. The incident wave from the feed is nearly planar (phase front radius of curvature is large relative to a wavelength).

6. The reflector is perfectly conducting.

7. The field expression of (2.3.1-1) is valid in the far field where $r >> 2\ D^2/\lambda$

Equation (2.3.1-1) can be written as [15, 16]

$$\vec{E} = -jk\eta \frac{e^{-jkr}}{4\phi r} (\bar{\bar{I}} - \hat{r}\,\hat{r}) \cdot \vec{T}(\theta,\phi) \qquad (2.3.1\text{-}2)$$

where

$$\vec{T}(\theta,\phi) = \int\int_{S_r} \vec{J}\, e^{jk\bar{r}'\cdot\hat{r}}\, dS \qquad (2.3.1\text{-}3)$$

or

$$\vec{E} = -jk\eta \frac{e^{-jkr}}{4\pi r} (T_\theta \hat{\theta} + T_\phi \hat{\phi}) \qquad (2.3.1\text{-}4)$$

It is only the $\theta$ and $\phi$ components which exist in the far field. They can be found from the rectangular components of $\bar{J}$ or $\bar{T}$ as follows

$$\begin{bmatrix} J_\theta \\ J_\phi \end{bmatrix} = [t] \begin{bmatrix} J_x \\ J_y \\ J_z \end{bmatrix}$$

$$\begin{bmatrix} T_\theta \\ T_\phi \end{bmatrix} = [t] \begin{bmatrix} T_x \\ T_y \\ T_z \end{bmatrix} \qquad (2.3.1\text{-}5)$$

where

$$[t] = \begin{bmatrix} \cos\theta\cos\phi & \cos\theta\sin\phi & -\sin\theta \\ -\sin\phi & \cos\phi & 0 \end{bmatrix} \qquad (2.3.1\text{-}6)$$

The integration in (2.3.1-3) can be greatly simplified by integrating over the projected aperture area $S_a$ (projection of $S_r$ on to the aperture xy-plane). If this is done by first ray tracing from the feed to the reflector aperture plane and then establishing equivalent currents with the resulting field components (only x and y components in this case) the GO/aperture field approximation results. However, we would like to avoid this approach. Galindo-Israel et al. [15, 16] found a way to evaluate (2.3.1-3) exactly with an aperture plane integration. This is done by introducing the Jacobian of the coordinate transformation from the reflector surface to the aperture plane:

$$C = \sqrt{1+(\partial f/\partial \rho')^2 + (\partial f/\partial \phi')^2/(\rho')^2} \qquad (2.3.1\text{-}7)$$

Then $\vec{T}$ can be evaluated on $S_a$ as

$$\vec{T} = \iint_{S_a} \vec{J}\, e^{jk\bar{r}'\cdot\hat{f}}\, C\, \rho' d\rho' d\phi' \qquad (2.3.1\text{-}8)$$

The function $\vec{JC}$ can be thought of as an "equivalent aperture distribution". It is not a physical distribution on the projected aperture such as the distribution derived strictly by ray tracing. [16] If this were so the kernel of (2.3.1-8) would be a Fourier transform kernel, which it is not. [16]

The basic radiation integral of (2.3.1-8) has now been developed and we next turn to providing further details on its evaluation. First we note that the Jacobian C equals the magnitude of the vector normal to the reflector surface:

$$N = -(\partial f/\partial x')\hat{x} - (\partial f/\partial y')\hat{y} + \hat{z} \qquad (2.3.1\text{-}9)$$

So

$$N = (\partial f/\partial x')^2 + (\partial f/\partial y')^2 + 1 = C \qquad (2.3.1\text{-}10)$$

The equivalent aperture distribution using the surface current density on the reflector surface from (2.3.1-1) is then

$$\begin{aligned} \vec{JC} &= \vec{JN} \\ &= 2\,\hat{n}\, N \times \vec{H}' = 2\,\vec{N} \times \vec{H}' \end{aligned} \qquad (2.3.1\text{-}11)$$

where $\vec{H}'$ is the magnetic field intensity incident on the lit portion of the reflector surface referenced to reflector coordinates. The radiation integral of (2.3.1-8) is then

$$\vec{T}(\theta,\phi) = \iint_{S_a} 2\,\vec{N} \times \vec{H}'(\vec{r}')\, e^{jk\vec{r}' \cdot \hat{r}}\, \rho' d\rho' d\phi' \qquad (2.3.1\text{-}12)$$

The exponential is evaluated as follows:

$$\begin{aligned} \vec{r}' \cdot \hat{r} &= (\hat{x}\,\rho'\cos\phi' + \hat{y}\,\rho'\sin\phi' + \hat{z}\,z') \\ &\quad \cdot(\hat{x}\sin\theta\cos\phi + \hat{y}\sin\theta\sin\phi + \hat{z}\cos\theta) \\ &= \rho'\cos\phi'\sin\theta\cos\phi + \rho'\sin\phi'\sin\theta\sin\phi + z'\cos\theta \\ &= \rho'\sin\theta\cos(\phi'-\phi) + r'\cos\theta'\cos\theta \end{aligned} \qquad (2.3.1\text{-}13)$$

So

$$\vec{T}(\theta,\phi) = \iint_{S_a} 2\,\vec{N} \times \vec{H}'(\vec{r}')\, e^{jkz'\cos\theta}\, e^{jk\rho'\sin\theta\cos(\phi'-\phi)}\, \rho'\, d\rho'\, d\phi' \qquad (2.3.1\text{-}14)$$

It remains to evaluate the surface field H' which arises from the feed antenna. The feed antenna has radiation pattern field components in feed coordinates $(r^\circ,\theta^\circ,\phi^\circ)$ given by

$$\begin{aligned} E_\theta &\propto U(\theta^\circ,\phi^\circ) \\ E_\phi &\propto V(\theta^\circ,\phi^\circ) \end{aligned} \qquad (2.3.1\text{-}15)$$

Since the reflector is assumed to be in the far field of the feed we can use spherical wave behavior with the pattern components of (2.3.1-15) to write the total electric field intensity expression of the feed antenna as

$$\vec{E}_s(r_s^\circ) = [U(\theta^\circ,\phi^\circ)\hat{\theta} + V(\theta^\circ,\phi^\circ)\hat{\phi}]\, \frac{e^{jkr^\circ}}{4\pi r^\circ} \qquad (2.3.1\text{-}16)$$

The corresponding magnetic field intensity is

$$\vec{H}_s(r_s^\circ) = [-V(\theta^\circ,\phi^\circ)\hat{\theta} + U(\theta^\circ,\phi^\circ)\hat{\phi}]\, \frac{e^{-jkr^\circ}}{4\pi\eta r^\circ} \qquad (2.3.1\text{-}17)$$

where the field is determined relative to the feed system (super 0) represented by spherical components (subscript s). This needs to be expressed in reflector (primed) Cartesian coordinates (superscript c). This is done by performing appropriate transformations between the feed and reflector systems. For completeness the expression is given below [17]:

$$H_c'(r') \rightarrow \begin{bmatrix} H'_x \\ H'_y \\ H'_z \end{bmatrix} =$$

$$\begin{bmatrix} A_{11} & A_{21} & A_{31} \\ A_{12} & A_{22} & A_{32} \\ A_{13} & A_{23} & A_{33} \end{bmatrix} \begin{bmatrix} \sin\theta^o \cos\phi^o & \cos\theta^o \cos\phi^o & -\sin\phi^o \\ \sin\theta^o \sin\phi^o & \cos\theta^o \sin\phi^o & \cos\phi^o \\ \cos\theta^o & -\sin\theta^o & 0 \end{bmatrix} \tag{2.3.1-18}$$

$$\begin{bmatrix} 0 \\ -V(\theta^o,\phi^o) \\ U(\theta^o,\phi^o) \end{bmatrix} \frac{e^{-jkr^o}}{4\pi\eta r^o}$$

The next chapter discusses in detail the transformation process and how it relates the feed position and illumination to the reflector surface. The above equation will be developed.

### 2.3.2 SUMMARY

The complexity of this development warrants a step-by-step summary. This summary serves to pull together the entire evaluation process

presented in the previous subsection of this chapter. The radiation integral of (2.3.1-14) is to be evaluated numerically, which is discussed in Section 3.4. The numerical integration process involves selecting points $(\rho',\phi')$ on $S_a$ and approximating the integral by summing integrand values at these points in some fashion. To find the integrand values one must work backwards to the feed as in the following steps.

1) Project the point $(\rho',\phi')$ in the aperture $S_a$ on to the reflector surface $S_r$ using

$$z' = \tilde{f}(\rho', \phi') = f(x', y') \qquad (2.3.2\text{-}1)$$

where f is a function describing the reflector surface.

2) Calculate the Cartesian coordinate position (x', y',z') of the reflector using a cylindrical to Cartesian coordinate component transformation.

$$\begin{aligned} x' &= \rho' \cos\phi' \\ y' &= \rho' \sin\phi' \\ z' &= z' \end{aligned} \qquad (2.3.2\text{-}2)$$

3) Calculate Cartesian coordinates of points on $S_r$ in source coordinates $(x^o,y^o,z^o)$ using a coordinate system transformation

$$\begin{bmatrix} x^o \\ y^o \\ z^o \end{bmatrix} = [A] \begin{bmatrix} x' - w_x^o \\ y' - w_y^o \\ z' - w_z^o \end{bmatrix} \qquad (2.3.2\text{-}3)$$

where [A] is the rotation matrix and $\bar{w}_c^o$ is the translation vector to be discussed in Chapter 3.

4) Convert the Cartesian point $(x^o,y^o,z^o)$ to its spherical

representation $(r^\circ,\theta^\circ,\phi^\circ)$ giving $\bar{r}_s^\circ$. This is used in (2.3.1-17) to obtain the H-fields at the reflector. (2.3.2-4)

5) Determine the equivalent H-field relative to the reflector system in Cartesian components using (2.3.1-18). This gives $\vec{H}_c'(\bar{r}')$. (2.3.2-5)

6) Determine the normal to the reflector surface using (2.3.2-6)

$$\vec{N} = -(\partial f/\partial x')\hat{x} - (\partial f/\partial y')\hat{y} + \hat{z} \qquad (2.3.2\text{-}6)$$

7) Find the equivalent aperture distribution using

$$\begin{aligned} 2\,\vec{N} \times \vec{H}_c' = 2\{&\hat{x}[N_y H_z' - N_z H_y'] \\ &+ \hat{y}[N_z H_x' - N_x H_z'] \\ &+ \hat{z}[N_x H_y' - N_y H_x']\} \end{aligned} \qquad (2.3.2\text{-}7)$$

8) Evaluate the components $T_x, T_y$, and $T_z$ of the integrand of (2.3.1-14) at $(\rho',\phi')$ in accordance with numerical integration routine selected. (2.3.2-8)

9) Find $T_\theta$ and $T_\phi$ using (2.3.1-5) (2.3.2-9)

10) Find the radiated field using

$$E = -jk\eta \frac{e^{-jkr}}{4\pi r}(T_\theta \hat{\theta} + T_\phi \hat{\phi}) \qquad (2.3.2\text{-}10)$$

# 3. THE REFLECTOR ANTENNA PROGRAM - RAP

In Section 2.3.2 the approach used in RAP was outlined. The method uses physical optics (PO) where the radiation integral is defined in the projected aperture of the reflector. The surface currents formed by geometrical optics (GO) techniques are obtained by a general reflector/feed transformation. Section 3.1 discusses all the necessary details of this transformation; it is used in Chapter 4 to develop the program MFRAP (Multiple Feed Reflector Antenna Program). Subsequent sections of this chapter provide details on the steps summarized in Section 2.3.2.

First, the geometry and general transformation technique is presented which develops into a reflector/feed application discussion (steps 1 through 5). Second, the feed pattern is described with emphasis on inclusion of polarization and appropriate interpolation methods. Third, the surface currents defined in the aperture plane are developed (steps 6 and 7). Fourth, a quick overview is given on the numerical evaluation of the radiation integral (steps 8 through 10). And finally, a summary of RAP test results are included showing the accuracy of the approach.

## 3.1 GEOMETRY

The choice of coordinate systems and other geometric formulations impacts greatly on the clarity, level of mathematical complexity, and solution difficulty. The following geometry was chosen based on these considerations. This approach follows that of Y. Rahmat-Samii [17] and is easily adapted to computers. The notation has been changed to be consistent with the reflector/feed geometry of RAP and to allow for expansion into the multi-element feed approach discussed in Chapter 4.

The geometry is based on general coordinate component and system transformations. Coordinate component transformations convert between Cartesian and spherical components within one coordinate system. Cylindrical components can also be obtained. The technique uses vector and matrix algebra. Subsection 3.1.1 discusses the transformation in full. Coordinate system transformations convert between two separate Cartesian coordinate systems. The technique is based on the one translation and three rotation approach first presented by Y. R. Samii [17]. Vectors and matrices are used. Both of the above transformation techniques are discussed in the following subsections.

### 3.1.1 COORDINATE COMPONENT TRANSFORMATION

The basic relations between Cartesian, cylindrical and spherical components is discussed. Position vectors defining a point in space and component vectors defining a vector at a point in space may be transformed with this technique. Notation is introduced that will be used in the next subsection.

The position vector $\bar{r}$ can be described by either Cartesian ($\bar{r}_c$), spherical ($\bar{r}_s$) and cylindrical ($\bar{r}_c$) components. Figure 3.1.1-1 shows the relation between Cartesian and spherical components. Cylindrical components are not presented in as much detail for they are not used as extensively as the others. The unit vectors of the Cartesian components are written as

$$\{\hat{c}\} = \{\hat{x},\ \hat{y},\ \hat{z}\}^t \qquad (3.1.1\text{-}1)$$

where the superscript t represents the transpose operator. The spherical and cylindrical components are written similarly as

$$\{\hat{s}\} = \{\hat{r},\ \hat{\theta},\ \hat{\phi}\}^t$$
$$\{\hat{c}\} = \{\hat{\rho},\ \hat{\phi},\ \hat{z}\}^t \qquad (3.1.1\text{-}2)$$

It can be shown that Cartesian and spherical components are related in general by the following transformation

$$\{\hat{s}\} = [{}_sT_c] \quad \{\hat{c}\} \qquad (3.1.1\text{-}3)$$

where transformation matrix $[{}_sT_c]$ is defined below:

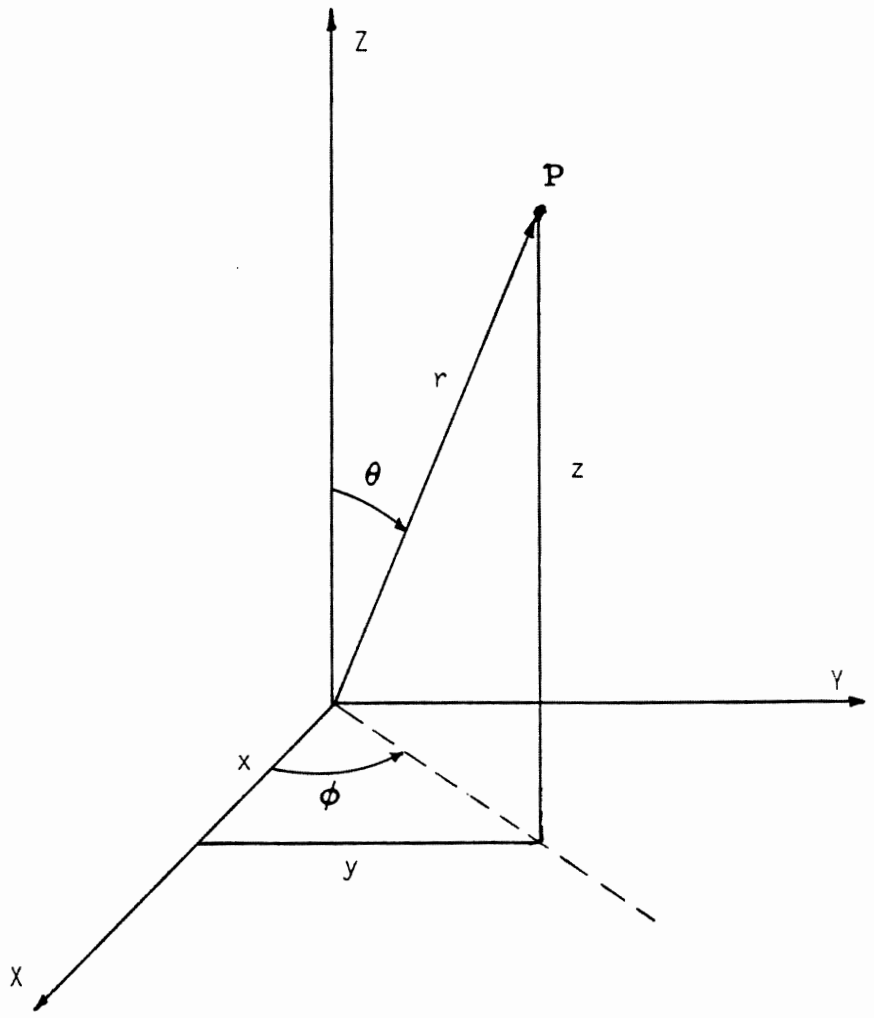


Figure 3.1.1-1 Cartesian (x, y, z) and Spherical (r, θ, ϕ) components describing point P.

$$\left[{}_{s}T_{c}\right] = \begin{bmatrix} \sin\theta\cos\phi & \sin\theta\sin\phi & \cos\theta \\ \cos\theta\cos\phi & \cos\theta\sin\phi & -\sin\theta \\ -\sin\phi & \cos\phi & 0 \end{bmatrix} \qquad (3.1.1\text{-}4)$$

Similarly, equation (3.1.1-3) can be written as

$$\begin{aligned} \{\hat{c}\} &= [{}_{s}T_{c}]^{-1} \{\hat{s}\} \\ &= [{}_{c}T_{s}] \{\hat{s}\} \end{aligned} \qquad (3.1.1\text{-}5)$$

to transform spherical to Cartesian components. Note

$$[{}_{s}T_{c}]\,[{}_{s}T_{c}]^{-1} = [I] \qquad (3.1.1\text{-}6)$$

such that, [I] is the identity matrix below

$$[I] = \begin{bmatrix} 1 & 0 & 0 \\ 0 & 1 & 0 \\ 0 & 0 & 1 \end{bmatrix}$$

It can be shown that equation (3.1.1.-6) is satisfied if

$$[{}_{c}T_{s}] = [{}_{s}T_{c}]^{-1} = [{}_{s}T_{c}]^{t}$$

Hence, from (3.1.1-4)

$$[{}_{c}T_{s}] = \begin{bmatrix} \sin\theta\cos\phi & \cos\theta\cos\phi & -\sin\theta \\ \sin\theta\sin\phi & \sin\theta\sin\phi & \cos\phi \\ \cos\theta & -\sin\theta & 0 \end{bmatrix} \qquad (3.1.1\text{-}7)$$

The unit vector relations of (3.1.1-3) and (3.1.1-5) are easily expanded to vector components by appropriate scalars. For example, an H-field can be represented in Cartesian components as

$$\vec{H}_{c} = H_{x}\hat{x} + H_{y}\hat{y} + H_{z}\hat{z}$$

and similarly for spherical components as

$$\vec{H}_s = H_r\hat{r} + H_\theta\hat{\theta} + H_\phi\hat{\phi}$$

The subscripts c and s represent the Cartesian and spherical system representations. The relations of equations (3.1.1-3) and (3.1.1-5) still hold such that

$$\vec{H}_c = [{}_cT_s]\,\vec{H}_s \qquad (3.1.1\text{-}8)$$

$$\vec{H}_s = [{}_sT_c]\,\vec{H}_c \qquad (3.1.1\text{-}9)$$

Note that cylindrical component vectors are not used in RAP so they were not introduced. However, cylindrical position vectors are used and can be represented by $\vec{r}_c$. Spherical ($\vec{r}_s$) and Cartesian ($\vec{r}_c$) position vectors are written similarly and are functions of the coordinate components of their respective systems. Table 3.1.1 defines the transformation between each of the three coordinate position vectors.

Concluding, transformations between Cartesian, spherical and cylindrical position vectors was obtained. In particular, Cartesian and spherical component vectors were related via a 3-by-3 matrix multiplication. These important relations are included in the next subsection where a transformation between two coordinate systems is introduced.

Table 3.1.1

Summary of Position Vector Transformations

| SPHERICAL | CARTESIAN | CYLINDRICAL |
|---|---|---|
| $\hat{S} = (\hat{r}, \hat{\theta}, \hat{\phi})$ | $\hat{c} = (\hat{x}, \hat{y}, \hat{z})$ | $\hat{\bar{c}} = (\hat{\rho}, \hat{\phi}, \hat{z})$ |
| $\bar{r}_s\ (r, \theta, \phi)$ | $\bar{r}_c\ (x, y, z)$ | $\bar{r}_c\ (\rho, \phi, z)$ |
| $\begin{bmatrix} r \\ \theta \\ \phi \end{bmatrix}$ | $= \begin{bmatrix} \sqrt{x^2 + y^2 + z^2} \\ \tan^{-1}\left(\frac{\sqrt{x^2 + y^2}}{z}\right) \\ \tan^{-1}\left(\frac{y}{z}\right) \end{bmatrix}$ | $= \begin{bmatrix} \sqrt{\rho^2 + z^2} \\ \tan^{-1}\left(\frac{\rho}{z}\right) \\ \phi \end{bmatrix}$ |
| $\begin{bmatrix} r\sin\theta\cos\phi \\ r\sin\theta\sin\phi \\ r\cos\theta \end{bmatrix}$ | $= \begin{bmatrix} x \\ y \\ z \end{bmatrix}$ | $= \begin{bmatrix} \rho\cos\phi \\ \rho\sin\phi \\ z \end{bmatrix}$ |
| $\begin{bmatrix} r\sin\theta \\ \phi \\ r\cos\theta \end{bmatrix}$ | $= \begin{bmatrix} \sqrt{x^2 + y^2} \\ \tan^{-1}\left(\frac{y}{x}\right) \\ z \end{bmatrix}$ | $= \begin{bmatrix} \rho \\ \phi \\ z \end{bmatrix}$ |

### 3.1.2 COORDINATE SYSTEM TRANSFORMATION

In general, two Cartesian coordinate systems can be related by one translation and three rotations. Note that the following transformation is for Cartesian systems; if the desired components are in either spherical or cylindrical form then they must be converted to their Cartesian counterpart. The component transformations developed in subsection 3.1.1 should be used.

The translation between the two systems is represented by a Cartesian translation (offset) vector whose tip and tail define the system origins. Figure 3.1.2-1 shows the reference (primed) and translated (super 0) systems positioned by the vector $\bar{w}_c^o$. The translation vector defines the position of the super 0 system in Cartesian components and is written as $\bar{w}_c^o = w_x^o\hat{x} + w_y^o\hat{y} + w_z^o\hat{z}$. The vector relationship between the two systems will be discussed with the assumption that the two systems are aligned (i.e. not rotated).

If the two coordinate systems are aligned with one another as shown in Figure 3.1.2-1, then the Cartesian position vectors are related by the following vector addition

$$\bar{r}_c' = \bar{w}_c^o + \bar{r}_c^o \qquad (3.1.2\text{-}1a)$$

where the superscripts (on $\bar{r}$) indicate to which system the Cartesian (subscript c) unit vectors are referenced. These can be written more descriptively as

$$\bar{r}_c^{\,\prime}\ \{\hat{x}',\ \hat{y}',\ \hat{z}'\}$$

$$\bar{r}_c^{\,o}\ \{\hat{x}^o,\ \hat{y}^o,\ \hat{z}^o\} \qquad (3.1.2\text{-}1b)$$

Note that because these systems are aligned the unit vectors have the same direction and may be equated giving

$$\hat{x}' = \hat{x}^o$$

$$\hat{y}' = \hat{y}^o$$

$$\hat{z}' = \hat{z}^o$$

Equation (3.1.2-1) becomes

$$\begin{bmatrix} x' \\ y' \\ z' \end{bmatrix} = \begin{bmatrix} w_x^o \\ w_y^o \\ w_z^o \end{bmatrix} + \begin{bmatrix} x^o \\ y^o \\ z^o \end{bmatrix} = \begin{bmatrix} w_x^o + x^o \\ w_y^o + y^o \\ w_z^o + z^o \end{bmatrix} \qquad (3.1.2\text{-}2)$$

In general, however, the translated coordinate system may be rotated with respect to the reference system. The rotation is described via three rotations. The angles formed by these rotations are known as Eulerian angles ($\alpha$, $\beta$, $\gamma$) [17]. These angles are used with the translation vector to finalize the transformation between the two Cartesian coordinate systems. The understanding of the Eulerian angles is important so the next paragraph will be used to define them.

The following Eulerian Angle definitions are written in the order in which the rotations should be performed. Angle $\alpha$ describes a counterclockwise rotation about the $z'$ (and $z^o$) axis looking down the $z'$ axis from $z' = +\infty$. Figure 3.1.2-2a shows the angle $\alpha$. The angle defines an imaginary line called the line of nodes (LCN) which lies along the $x^o$

axis. This definition will become more apparent as the discussion continues. Angle β describes a counterclockwise rotation about the $x^o$-axis (and line of nodes) looking down the $x^o$-axis from $x^o = +\infty$. The $z^o$ and $y^o$ axes are now off the z' and y' axes, whereas $x^o$ still remains on the line of nodes. Figure 3.1.2-2b shows the angle β. Angle ɣ describes a counterclockwise rotation about the $z^o$-axis from $z^o = +\infty$. The $x^o$-axis has moved off the line of nodes. Figure 3.1.2-2c shows the angle ɣ. At this point the line of nodes becomes apparent. This line describes the intersection of the $x^oy^o$ and x'y' planes. Before proceeding into the mathematical formulations discussed next, it will be helpful to picture the primed and super o coordinates as the reflector and feed systems, respectively. The usefulness of the technique is presented in the next subsection.

The three rotations described above align the two Cartesian system unit vectors as

$$\{\hat{c}^o\} = [{}^oA'] \{\hat{c}'\} \qquad (3.1.2\text{-}3)$$

and can therefore be used to align vector components as

$$\vec{H}^o_c = [{}^oA'] \vec{H}'_c \qquad (3.1.2\text{-}4)$$

where $[{}^oA']$ is the rotation matrix obtained from the multiplication below

$$[{}^{o}A'] = \begin{bmatrix} \cos\gamma & \sin\gamma & 0 \\ -\sin\gamma & \cos\gamma & 0 \\ 0 & 0 & 1 \end{bmatrix} \qquad (3.1.2\text{-}5a)$$

$$\begin{bmatrix} 1 & 0 & 0 \\ 0 & \cos\beta & \sin\beta \\ 0 & -\sin\beta & \cos\beta \end{bmatrix} \begin{bmatrix} \cos\alpha & \sin\alpha & 0 \\ -\sin\alpha & \cos\alpha & 0 \\ 0 & 0 & 1 \end{bmatrix}$$

The 3 by 3 matrix formed above is given by $[A_{ij}]$ where i and j define the row (i) and column (j) positions below.

$$A_{11} = \cos\gamma \cos\alpha - \sin\gamma \cos\beta \sin\alpha$$

$$A_{12} = \cos\gamma \sin\alpha + \sin\gamma \cos\beta \cos\alpha$$

$$A_{13} = \sin\gamma \sin\beta$$

$$A_{21} = -\sin\gamma \cos\alpha - \cos\gamma \cos\beta \sin\alpha \qquad (3.1.2\text{-}5b)$$

$$A_{22} = -\sin\gamma \sin\alpha + \cos\gamma \cos\beta \cos\alpha$$

$$A_{23} = \cos\gamma \sin\beta$$

$$A_{31} = \sin\beta \sin\alpha$$

$$A_{32} = -\sin\beta \cos\alpha$$

$$A_{33} = \cos\beta$$

Note that with $\alpha = \beta = \gamma = 0$, the rotation matrix becomes the identity matrix and no rotation is performed.

Matrix algebra can be used on equations (3.1.2-3) and (3.1.2-4) giving

$$\{\hat{c}'\} = [{}^{o}A']^{-1} \{\hat{c}^{o}\} \qquad (3.1.2\text{-}6)$$

and

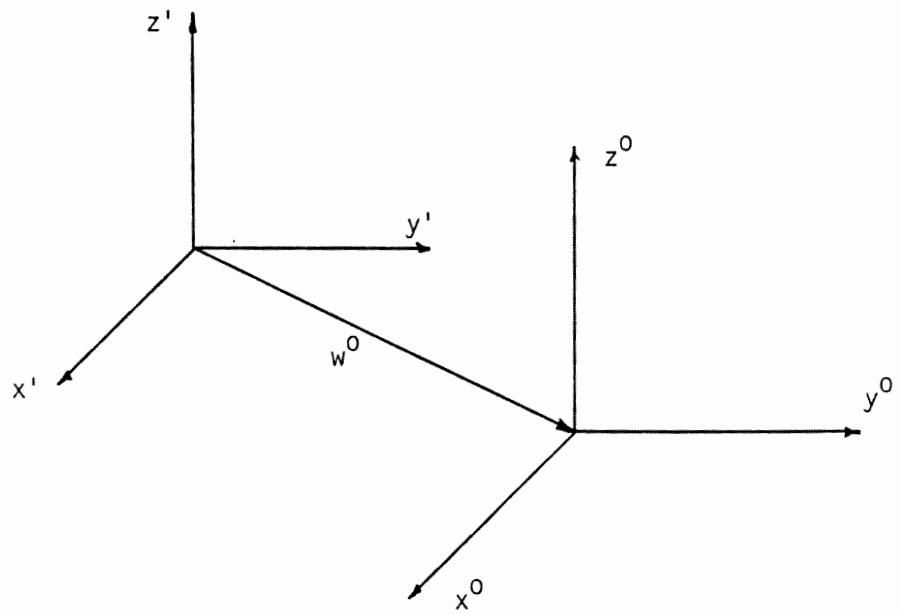


Figure 3.1.2-1. Translation between two Cartesian coordinate systems.

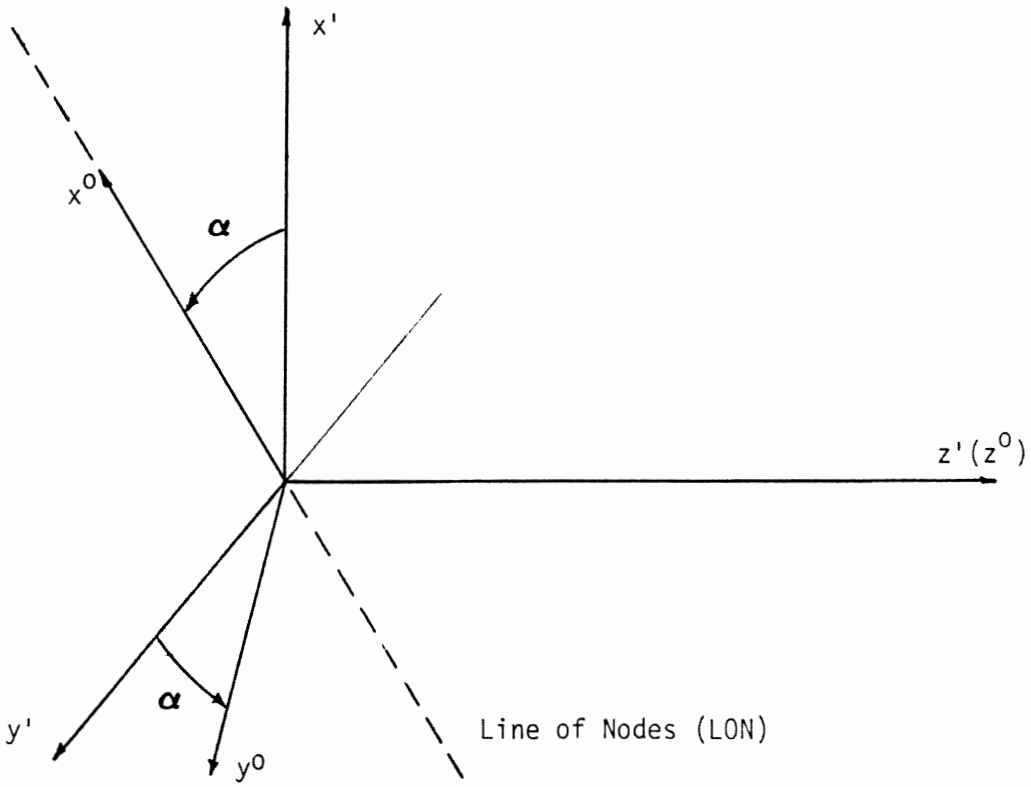


Figure 3.1.2-2a. Eulerian Angle α, counterclockwise rotation about the z' (and $z^o$) axis as looking down the z' axis from z' = +∞. Defines the Line of Nodes. (LON).

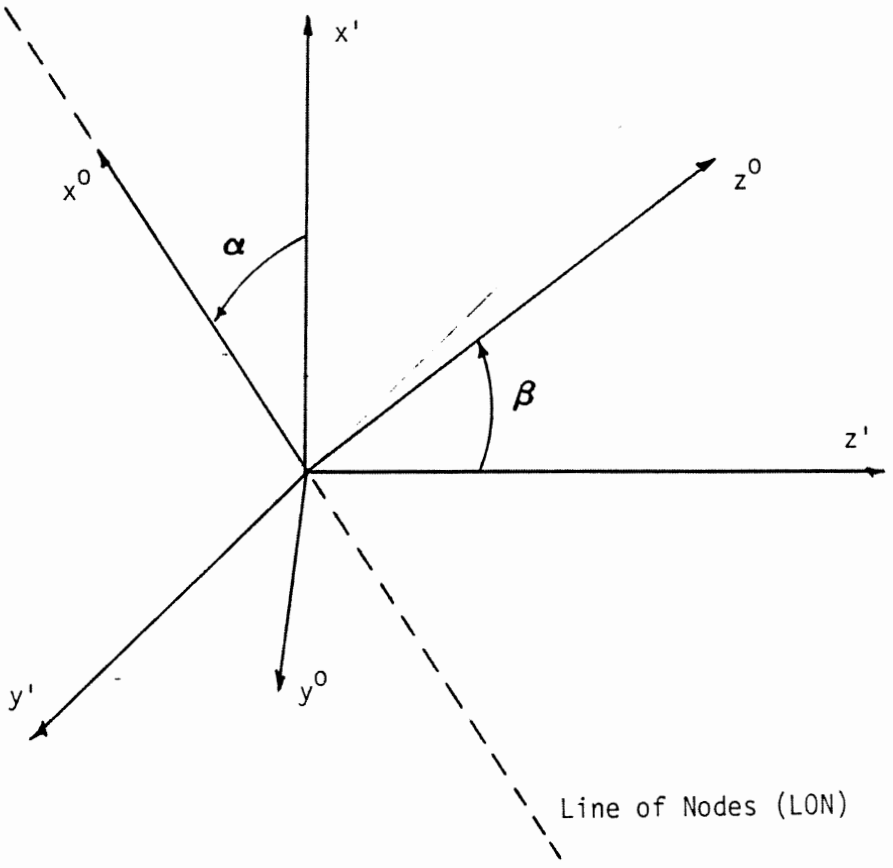


Figure 3.1.2-2b. Eulerian Angle β, counterclockwise rotation about $x^o$ (and LON) axis as looking down the $x^o$ axis from $x^o = +\infty$.

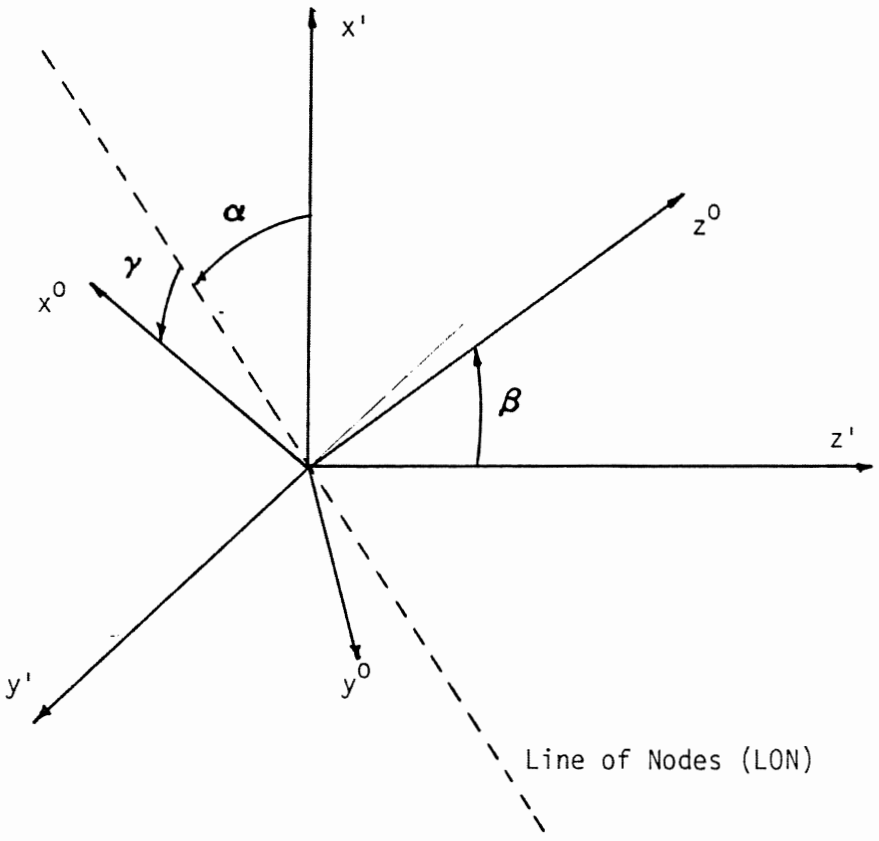


Figure 3.1.2-2c. Eulerian Angle $\gamma$, counterclockwise rotation about the $z^o$ axis as looking down the $z^o$ axis from $z^o = +\infty$.

$$\vec{H}'_c = [{}^oA']^{-1} \vec{H}^o_c \qquad (3.1.2\text{-}7)$$

where

$$[{}^oA'] [{}^oA']^{-1} = [I]$$

as seen in equation (3.1.1-6).

Note the following relation

$$['A^o] = [{}^oA']^{-1} = [{}^oA']^t \qquad (3.1.2\text{-}8)$$

allows convenient rotation from one system to another. The methods behind combining translation and rotation are presented next.

Suppose two Cartesian coordinate systems are translated and rotated with respect to one another. This is a very practical example where the primed system represents the reflector system and the super o system represents the feed system. In this case, it is posed that the feed is offset (translated) to produce a scanned far-field beam. And to maximize aperture efficiency, the feed is rotated with Eulerian angles $\alpha,\beta,\gamma$ so as to point the feed radiation pattern towards the reflector. The above example gives a quick understanding of how useful this translation and rotation approach is for relating two different coordinate systems. The next subsection describes how the technique is done mathematically.

### 3.1.3 TRANSFORMATION APPLICATION

The coordinate component and coordinate system transformations discussed in the previous sections will be applied here to form the

approach used in RAP. As discussed earlier, it is often helpful to describe individual items such as feeds, surfaces and radiation patterns in their own coordinate systems. The transformations developed here allow the individual systems to be easily related to each other. Position and component vectors need transformation and both will be discussed next.

The feed radiation pattern illuminates the reflector surface. This illumination is represented by an outward traveling spherical phase front where it is assumed the reflector is in the far-field. The spherical phase front is most easily described by a spherical system. On the other hand, the reflector surface is best described by a cylindrical system. The problem is to find the magnitude and phase of the feed illumination on the reflector surface and at the same time allow for arbitrary feed location and rotation. This serves as an introduction to relating the coordinate transformations to a specific application. At the same time, the steps 1) through 5) in the summary presented in Subsection 2.3.2 will be obtained.

The process starts where it is assumed that the function defining the reflector surface location is given by $z' = \tilde{f}(\rho',\phi')$. Thus the cylindrical position vector $\bar{r}_c'$ is known, defining a point in reflector coordinates. Step 2.3.2-1 is completed. The cylindrical components are then converted to their Cartesian counterparts using Table 3.1.1 thus completing Step 2.3.2-2. This gives

$$\bar{r}_c' = \begin{bmatrix} x' \\ y' \\ z' \end{bmatrix} = \begin{bmatrix} \rho' \cos\phi' \\ \rho' \sin\phi' \\ z' \end{bmatrix} \qquad (3.1.3\text{-}1)$$

The translation vector $(\bar{w}_c^o)$ defining the feed location and the Eulerian angles $(\alpha,\beta,\gamma)$ defining the feed orientation are given. The Eulerian angles are used to find the rotation matrix $[^oA']$ by equation (3.1.2-5). Now by applying equations (3.1.2-2) and (3.1.2-4) the Cartesian components relative to the feed system $(r_c^o)$ can be obtained. This is Step 2.3.2-3 given as

$$\bar{r}_c^o = [^oA'] \; (\bar{r}_c' - \bar{w}_c^o) \qquad (3.1.3\text{-}2)$$

and written in component form as

$$\begin{bmatrix} x^o \\ y^o \\ z^o \end{bmatrix} = [^oA'] \begin{bmatrix} x' - w_x^o \\ y' - w_y^o \\ z' - w_z^o \end{bmatrix} \qquad (3.1.3\text{-}3)$$

The spherical components of $(r_c^o)$ above are easily obtained by applying formula from Table 3.1.1 giving

$$r = \sqrt{x^2 + y^2 + z^2}$$

$$\theta = \tan^{-1} \frac{\sqrt{x^2 + y^2}}{z}$$

$$\phi = \tan^{-1}\left(\frac{y}{z}\right)$$

where the super o was dropped for the time being. Now, given the point $\bar{r}_s^o$ then the H-fields from the feed at that point can be obtained from (2.3.1-17) giving

$$\vec{H}_s^o(\bar{r}_s^o) = [-V(\theta^o,\phi^o)\,\hat{\theta} + U(\theta^o,\phi^o)\,\hat{\phi}]\,\frac{e^{-jkr^o}}{4\pi\eta r^o} \qquad (3.1.3\text{-}4)$$

Step (2.3.2-4) is complete.

The problem now remains to represent the feed field $\vec{H}_s^o$ in terms of reflector Cartesian components thereby forming $\vec{H}_c'$. First, the field $\vec{H}_s^o$ needs conversion to Cartesian components so that the coordinate system transformation can take place. This is done by the component transformation of (3.1.1-8)

$$\vec{H}_c^o = [{}_cT_s]\,\vec{H}_s^o \qquad (3.1.3\text{-}5)$$

where $[{}_cT_s]$ is (3.1.1-7). The Cartesian components are easily rotated with the help of the rotation matrix $[{}^oA']$ and equations (3.1.2-7) and (3.1.2-8) giving

$$\vec{H}_c' = [{}^oA']^t\,\vec{H}_c^o \qquad (3.1.2\text{-}5)$$

where $[{}^oA']$ is (3.1.2-5). The above two steps can be combined into a single equation written as

$$\vec{H}_c' = [{}^oA']^t\,[{}_sT_c]^t\,\vec{H}_s^o \qquad (3.1.3\text{-}15)$$

This completes step 2.3.2-5 where equation (2.3.1-18) is formed when (3.1.3-15) is written in components. It is important to realize that $\vec{H}_s^o$

and $\vec{H}_c'$ represent identical vectors; however, they are referenced to different systems and unit vector notations.

The first five steps of the summary presented in subsection 2.3.2 were obtained. It now remains to find the equivalent aperture distribution and evaluate the radiation integral. First however, it will be both informative and useful to examine how the feed pattern is described. Specifically, polarization and interpolation is studied. This will "close the loop' on the feed field description allowing a succinct presentation of MFRAP in the next chapter.

## 3.2 FEED PATTERN DESCRIPTION

The feed antenna radiation pattern is one of the important variables in reflector design. For maximum directivity the feed pattern would uniformly (both magnitude and phase) illuminate the reflector surface and abruptly cutoff beyond the reflector edge. This requires an ideal inverse spherical spreading loss pattern. This condition maximizes both illumination and spillover efficiencies, but with -17.6 dB side lobes [18]. The feed pattern magnitude must be tapered to lower sidelobes. Other designs require adjustments in phase to produce maximum directivity for scanned feed designs. Obviously there are infinitely many reflector requirements and just as many feed designs. Hence a simple, efficient,

and complete method of feed pattern description is needed to meet the many reflector design requirements.

A method is discussed which allows the description of an individual element radiation pattern. The technique uses principal plane E-field theta and phi components. Simple interpolations are performed to find values of the E-field components between known principal planes. The system is self-contained in the sense that it can be described within its own coordinate system. In other words, polarization is introduced and interpolation is performed without reference to another system. The self-contained constraint is important because as discussed in Chapter 4 many feed elements will be superimposed producing an array type radiation pattern. The individual elements must remain independent of one another to insure that their locations and rotations also produce independent patterns.

Another important quality of the method is its ability to employ both linear and circular polarizations. The reflector can therefore be analyzed for any polarization sense. Note however that when illuminated by right hand circular polarization; left hand circular polarization is reflected [19].

The ability to accept and analyze measured feed pattern data (both co- and cross-pol) is also important. This technique allows measured data to be used directly in the feed description. (Note however that circular polarization must have its 90 degree phase lead (or lag) removed from the data because it is introduced within RAP.) Analytically predicted feed

patterns can also be used with this technique. A short presentation will be made on the theory concerning the feed pattern description followed by subsections discussing the polarization and interpolation methods.

Feed radiation patterns are usually described in spherical coordinates in which the principal plane E-fields are known. Usually, the r component of this field is assumed zero implying the reflector is in the far field of the feed. However this field can be written in general as

$$\vec{E}_s^o = \begin{Bmatrix} E_r^o(r^o,\theta^o,\phi^o)\ \hat{r} \\ E_\theta^o(r^o,\theta^o,\phi^o)\ \hat{\theta} \\ E_\phi^o(r^o,\theta^o,\phi^o)\ \hat{\phi} \end{Bmatrix} \qquad (3.2\text{-}1)$$

where the subscript represents spherical components and the superscript indicates feed system.

Removing the $\hat{r}$ dependence and assuming the reflector is in the far-field of the feed ($E_r = 0.$), gives

$$\vec{E}_s^o = [U(\theta^o,\phi^o)\hat{\theta} + V(\theta^o,\phi^o)\hat{\phi}]\ \frac{e^{-jkr^o}}{4\pi r^o} \qquad (3.2\text{-}2)$$

The above U and V represent actual $\theta$ and $\phi$ components for a measured feed system. The above far-field restriction forms a TEM wave in which the H-field can be obtained as [20],

$$\vec{H}_s^o(\vec{r}_s^o) = [-V(\theta^o,\phi^o)\ \hat{\theta} + U(\theta^o,\phi^o)\ \hat{\phi}]\ \frac{e^{-jkr^o}}{4\pi\eta r^o} \qquad (3.2\text{-}3)$$

where $\eta$ represents the intrinsic impedance of the medium. The feed H-field has now been written in terms of the E-field, however to be completely general $\bar{H}_s^o$ can be written as

$$\vec{H}_s^o(\bar{r}_s^o) = \begin{Bmatrix} H_r^o\ (r^o,\theta^o,\phi^o)\ \hat{r} \\ H_\theta^o\ (r^o,\theta^o,\phi^o)\ \hat{\theta} \\ H_\phi^o(r^o,\theta^o,\phi^o)\ \hat{\phi} \end{Bmatrix} \qquad (3.2\text{-}4)$$

A general representation of the feed pattern has been developed as a function of feed coordinates only. The interpolation methods to be described use the principal plane patterns to represent the feed. This is by no means the best way but the approximation is good for highly directive feed elements such as horns or open-ended wave-guides. [19] The method is an extension of most published techniques because cross polarization can be included; most methods treat only co-polarized patterns. The type of interpolation to be performed is based on the desired polarization state. So a brief discussion of polarization is made as an introduction to the interpolation subsection.

### 3.2.1 POLARIZATION

Polarization was one of the two major obstacles encountered in the development of this code. (For those interested, the coordinate transformation was the other.) So it is only fitting to devote some time

to this problem. So you ask, what is the problem? Well, there are too many ways to introduce polarization into the feed. Thank goodness Ludwig's third definition [21] has become a standard accepted by many researchers. This technique is also based on the third definition.

The most concise and complete method available with both polarization and interpolation properties is that of P.T. Lam [19]. The technique uses three real valued polarization parameters (a, b, $\psi$) to define the four practical polarization states, namely: vertical ($x^o$ directed), horizontal ($y^o$ directed), right-hand circular (RHC) and left-hand circular (LHC). And at the same time has adequate interpolatory capability for ideal (zero cross-pol) feed patterns. An equivalent method is given below where notation was changed to be consistent with popular polarization formulations [22].

The feed E-field is given by the proportionality

$$\vec{E}_s^{\,o}(\vec{r}^{\,o}) \sim [\hat{\theta}\, U(\theta^o)\, (\cos\gamma \cos\phi^o + e^{j\delta^o} \sin\gamma \sin\phi^o) \qquad (3.2.1\text{-}1)$$

$$+ \hat{\phi} V(\theta^o)(-\cos\gamma \sin\phi^o + e^{j\delta^o} \sin\gamma \cos\phi^o)]$$

The values of the polarization parameters $\gamma$ and $\delta^o$ are listed in Table 3.2.1 for popular feed polarization states

Table 3.2.1
Polarization States

| State | $\gamma$ | $\delta^\circ$ |
|---|---|---|
| Linear (x) | 0 | 0 |
| Linear (y) | 90° | 0 |
| RHC | 45° | -90° |
| LHC | 45° | 90° |

The polarization state of the wave reflected from the main reflector must be related to the incident (feed) polarization state. This is done by applying Ludwig's third definition to the far field radiation patterns. The co- and cross- polarized unit vectors of the secondary pattern are given as [19, 1, 22].

$$\hat{e}_{co} = \hat{\theta}\,(+e^{j\delta}\cos\gamma\,\cos\phi + \sin\gamma\,\sin\phi) + \hat{\phi}\,(-e^{j\delta}\cos\gamma\,\sin\phi + \sin\gamma\,\cos\phi)$$

$$\hat{e}_{cr} = \hat{\theta}\,(\cos\gamma\,\sin\phi + e^{-j\delta}\sin\gamma\,\cos\phi) + \hat{\phi}(\cos\gamma\,\cos\phi - e^{-j\delta}\sin\gamma\,\sin\phi)$$

where $\hat{e}_{co} \cdot \hat{e}_{co}^{*} = 1$, $\hat{e}_{co} \cdot \hat{e}_{cr} = 0$. The secondary wave polarization parameter $\delta$ is related to the incident wave parameter $\delta^\circ$ by the phase change (180°) after reflection. This leads to

$$\delta = \delta^\circ + \pi$$

It was assumed above that a single reflection took place where all linear polarized components are changed in phase by 180°. A dual reflector

system would produce a 360° phase change. Other geometries are possible and the phase change should be included as required [19].

A different technique was developed independently and used in RAP. The method treats polarization and interpolation separately allowing analysis of feed patterns with finite cross-pol. This technique assumes that only three feed polarizations exist, namely: linear ($x^\circ$-directed), RHC and LHC. The feed polarization is introduced in the subroutine HFIELD where the linear polarization is fixed in the $x^\circ$ direction by a quadrant test. Essentially, the representation of Lam is obtained for linear (x) polarization giving

$$\vec{E}_s^{\,o} \sim [\hat{\theta}\, U(\theta^o)\cos\phi - \hat{\phi}\, V(\theta^o)\sin\phi^o]$$

Circular polarization is introduced as

$$\vec{E}_s^{\,o} \sim [\hat{\theta}\ (U(\theta^o)\, e^{js\phi^o}\frac{1}{\sqrt{2}}) + \hat{\phi}\ (V(\theta^o)\, js\, e^{js\phi^o}\frac{1}{\sqrt{2}})]$$

where

$s = -1$ for RHC
$\quad +1$ for LHC.

The far field co- and cross-polarized unit vectors for linear polarization are

$$\hat{e}_{co} = \hat{\theta}\cos(\tau - \phi) + \hat{\phi}\sin(\tau - \phi)$$
$$\hat{e}_{cr} = \hat{\theta}\sin(\tau + \phi) + \hat{\phi}\cos(\tau + \phi)$$

where

$\tau = 0^\circ$ for vertical polarization (x)
$\tau = 90^\circ$ for horizontal polarization (y)

Note that the Eulerian angle $\gamma$ (not to be confused with polarization angle $\gamma$) is used to rotate the feed $x^\circ$ unit vector to align with the $\hat{e}_{co}$ ($\tau = 0^\circ$ or $90^\circ$) unit vector. So theoretically $\gamma$ and $\tau$ could be related allowing infinite number of linear polarizations (i.e. not just vertical or horizontal). The circular polarized far field unit vectors are given as

$$\hat{e}_{co} = \hat{\theta}\left(\frac{-s}{\sqrt{2}} j e^{js\phi}\right) + \hat{\phi}\left(\frac{1}{\sqrt{2}} e^{js\phi}\right)$$

$$\hat{e}_{cr} = \hat{\theta}\left(\frac{s}{\sqrt{2}} j e^{-js\phi}\right) + \hat{\phi}\left(\frac{1}{\sqrt{2}} e^{-js\phi}\right)$$

where
$s = -1$ for incident RHC.
$= +1$ for incident LHC.

Undoubtedly, the method developed by P. T. Lam and the method developed for RAP are equivalent. The two were given for completeness.

### 3.2.2 INTERPOLATION

If an analytical function representation is available for the feed pattern, numerical calculations are rather simple. As points in the aperture are traced back to the reflector during the radiation integral

process corresponding feed pattern values can be evaluated from the feed pattern function using feed coordinate values. It is equally simple to perform the integration over the feed pattern to find gain and efficiency values.

On the other hand, frequently it is desired to input measured feed pattern information. Most often only principal plane pattern data are known. Then some interpolation procedure must be used to find intermediate values. Several approaches are possible. Often, the interpolating polynomial and the desired polarization state of the feed can be combined into a solitary equation (see equation 3.2.1-1). The approach taken by RAP was to separate the polarization and interpolating functions. This allows the cross-polarized component (usually small) for the feed to be included in the feed pattern description. In this section we describe the approach used in RAP.

Suppose that principal plane patterns

$U(\theta,\phi = 0°)$ and $V(\theta,\phi = 0°)$

$U(\theta,\phi = 90°)$ and $V(\theta,\phi = 90°)$

$U(\theta,\phi = 180°)$ and $V(\theta,\phi = 180°)$

$U(\theta,\phi = 270°)$ and $V(\theta,\phi = 180°)$

are known where the angles $\theta$ and $\phi$ are defined in the feed system. The problem is then to interpolate to find U* and V* values at any $(\theta^*,\phi^*)$ point as shown in Figure 3.2.2-1. The order of the interpolation is to interpolate along the principal planes (constant $\theta$) to find U and V for

the desired $\theta^*$ coordinate and then to interpolate in $\phi$ (for constant $\phi$) using the new U and V values. The result is a value for U and V at $(\theta^*,\phi^*)$.

Usually many points are known along measured phi-cuts, in this case principal planes. For this reason, a linear interpolation scheme is used to find U and V at $\theta^*$. Note two interpolations are needed, one at each principal plane as shown in Figure 3.2.2-2.

The second step in the interpolation process is to interpolate along constant $\theta^*$ as shown in Figure 3.2.2-3. In contrast to $\theta$ interpolation this $\phi$ interpolation has few known points. Typically only two points are known, one in each principal plane. Therefore we choose the interpolation scheme to match the feed polarization (linear or circular). These interpolators are discussed in the following paragraphs.

Circular Polarization

The underlying assumption of the circular polarization interpolator is that U and V are fairly constant in $\theta$. Therefore, a linear interpolation is used to find the U and V values at $(\theta^*,\phi^*)$. The form of the linear interpolator is

$$(R_1-R^*)/(R_1-R_2) = (\phi_1-\phi^*)/(\phi_1-\phi_2) \qquad (3.2.2\text{-}1)$$

where R is a 'dummy' variable standing for either U or V. The linearly interpolated value $R^*$ can be solved for explicitly and then can be used in the feed pattern description.

Linear Polarization

The pattern characteristics of a linear feed pattern can be described by cosines and sines. Hence a trigonometric polynomial is used to interpolate the feed pattern in $\phi^*$. The method of undetermined coefficients is used to implement this trigonometric polynomial in which a Vandermonde matrix is formed as below [23].

$$\begin{bmatrix} \cos \phi_1 & \sin \phi_1 \\ \cos \phi_2 & \sin \phi_2 \end{bmatrix} \begin{bmatrix} C_1 \\ C_2 \end{bmatrix} = \begin{bmatrix} R_1 \\ R_2 \end{bmatrix} \qquad (3.2.2\text{-}2)$$

The values of $\phi_1$ and $\phi_2$ stand for the principal plane values of $\phi$ used to find $R_1$ and $R_2$. Note that $R_1$ and $R_2$ represent either U or V. The constants $C_1$ and $C_2$ are found by performing

$$\begin{bmatrix} C_1 \\ C_2 \end{bmatrix} = \begin{bmatrix} \cos \phi_1 & \sin \phi_1 \\ \cos \phi_2 & \sin \phi_2 \end{bmatrix}^{-1} \begin{bmatrix} R_1 \\ R_2 \end{bmatrix} \qquad (3.2.2\text{-}3)$$

These constants are then used to find U or V with the following trigonometric function

$$R^* = C_1 \cos \phi^* + C_2 \sin \phi^* \qquad (3.2.2\text{-}4)$$

The result from this is then used in the feed pattern description.

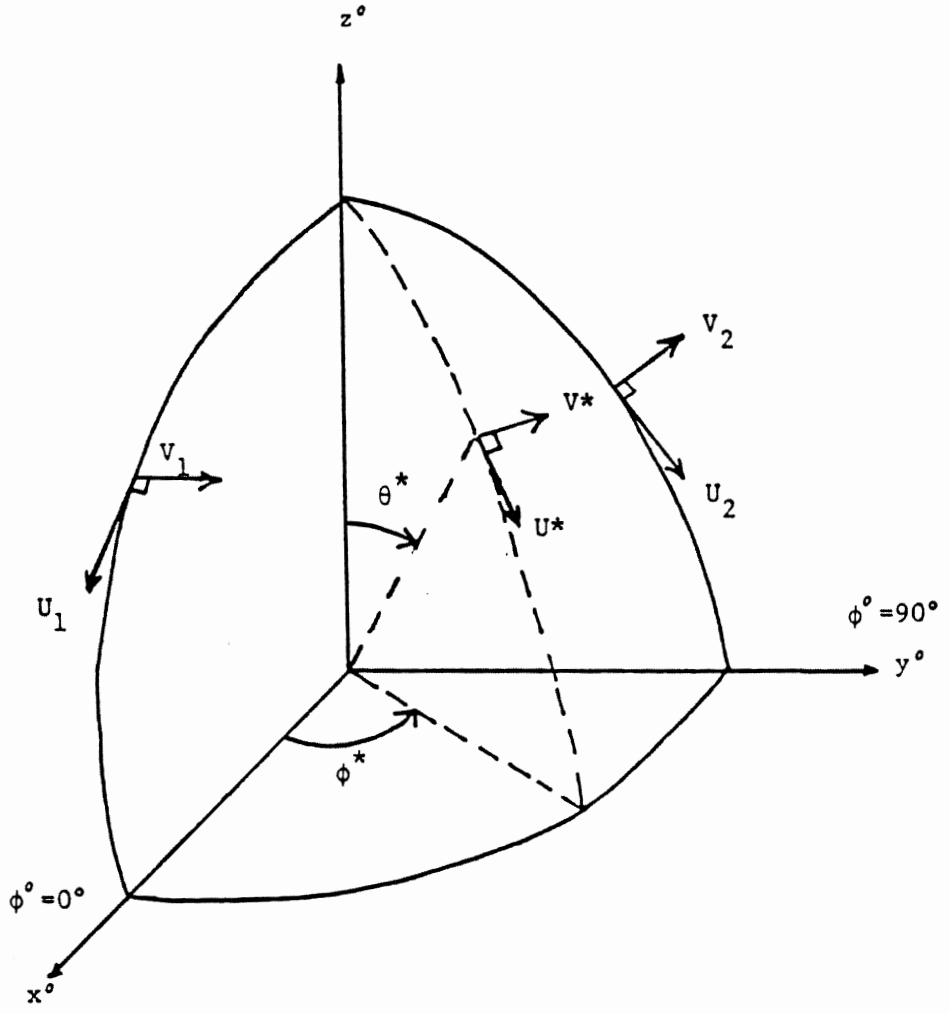


Figure 3.2.2-1. Interpolation at point (θ*, φ*) giving U* and V*.

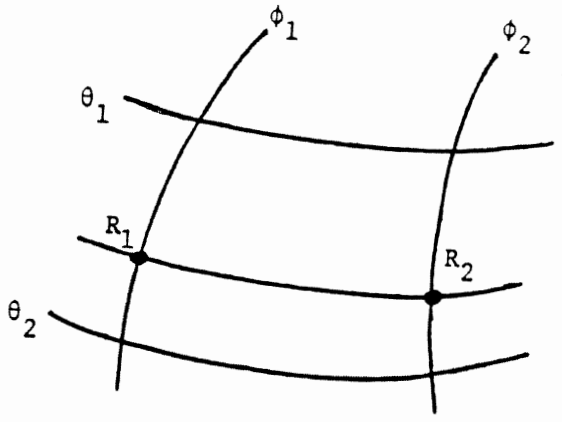


Figure 3.2.2-2 Linear interpolations along constant $\phi_1$ and $\phi_2$ curves giving values $R_1$ and $R_2$.

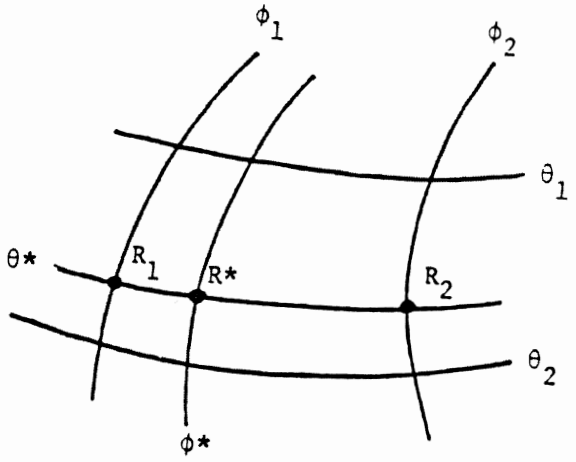


Figure 3.2.2-3. Interpolation along a constant $\theta^*$ giving $R^*$.

To illustrate, suppose we wish to interpolate in the first quadrant. Then $\phi_1 = 0$ and $\phi_2 = 90°$, and solving (3.2.2-3) gives $C_1 = R_1$ and $C_2 = R_2$. So (3.2.2-4) gives

$$U = U_1 \cos \phi^* + U_2 \sin \phi^*$$
$$V = V_1 \cos \phi^* + V_2 \sin \phi^* \qquad (3.2.2\text{-}5)$$

Note that although (3.2.2-3) is restricted to $\phi_1$, $\phi_2$ values along principal planes, it is used in each quadrant allowing asymmetrical feed patterns. This formulation also permits cross polarization in the feed.

Proceeding further with the illustration consider a purely linearly y-polarized feed. Then $U_1 = 0$ and $V_2 = 0$ giving (from 3.2-2)

$$\vec{E}_s^o(\bar{r}_s^o) = \frac{e^{-jkr}}{4\pi r} [U_2 \sin\phi^* \hat{\theta} + V_1 \cos\phi^* \hat{\phi}] \qquad (3.2.2\text{-}7)$$

This agrees with the result given by Kildal [24, eqn. (4)] and that given by equation (3.2.1-1).

## 3.3 EQUIVALENT CURRENT GENERATION

The technique used in RAP forms an aperture integral over equivalent surface currents. These projected currents are termed equivalent because they have their support on the reflector surface and contain exactly the same information as the surface currents [15]. The equivalent aperture distribution was formed in subsection 2.3.1 where the Jacobian of the

transformation between the reflector surface and projected aperture was introduced.

The Jacobian was defined by equation (2.3.1-7) as

$$C = \sqrt{1 + \left(\frac{\partial \tilde{f}}{\partial \rho'}\right)^2 + \left(\frac{\partial \tilde{f}}{\partial \phi'}\right)^2 \left(\frac{1}{\rho'}\right)^2} \qquad (3.3\text{-}1)$$

which when introduced into the physical optics radiation integral allowed the integration to be performed over the reflector projected aperture. The equivalent surface currents $\bar{J}C$ where formed. Recalling,

$$\vec{J} = 2\,\hat{n} \times \vec{H}_c' \qquad (3.3\text{-}2)$$

where $\hat{n}$ is the unit normal at the reflector surface given by

$$\hat{n} = \frac{\vec{N}}{N} \qquad (3.3\text{-}3)$$

$\vec{N}$ is the vector normal

$$\vec{N} = -\frac{\partial f}{\partial x'}\hat{x} - \frac{\partial f}{\partial y'}\hat{y} + 1\hat{z} \qquad (3.3\text{-}4)$$

and N is the magnitude

$$N = \sqrt{\left(\frac{\partial f}{\partial x'}\right)^2 + \left(\frac{\partial f}{\partial y'}\right)^2 + 1} \qquad (3.3\text{-}5)$$

It was then noted that the Jacobian equals the magnitude of the vector normal so that $\bar{J}C$ reduces to

$$\bar{\tilde{J}} = \bar{J}C = \bar{J}N = 2\,\vec{N} \times \vec{H}_c' \qquad (3.3\text{-}6)$$

which is equation (2.3.1 - 11). Performing the vector cross product gives for $\bar{\tilde{J}}(\bar{r}')$

$$\begin{bmatrix} \tilde{J}_x \\ \tilde{J}_y \\ \tilde{J}_z \end{bmatrix} = 2 \begin{bmatrix} N_y H_z' - N_z H_y' \\ N_z H_x' - N_x H_z' \\ N_x H_y' - N_y H_x' \end{bmatrix} \qquad (3.3\text{-}7)$$

The summary steps of 6) and 7) in Subsection 2.3.2 have been completed.

## 3.4 RADIATION INTEGRAL EVALUATION

The radiation integral formed in Subsection 2.3.1 is given explicitly by equation (2.3.1-14). It is this integral that requires evaluation.

$$\vec{T}_c(\theta,\phi) = \iint_{S_a} \vec{\tilde{J}}(\bar{r}')\, e^{jkz'\cos\theta} \, e^{jk\rho'\sin\theta\cos(\phi'-\phi)} \rho' \, d\rho' \, d\phi' \qquad (3.4\text{-}1)$$

where $\vec{\tilde{J}}(\bar{r}')$ are the equivalent surface currents of Section 3.3. Note that the subscript c on $\bar{T}_c$ is a reminder that this is a Cartesian representation.

Many numerical integration methods were investigated [1] resulting in the choice of a back-to-back $\rho'$, $\phi'$ Gaussian-Legendre technique. Later, a composite feature was added for the $\phi'$ integration. This produces a number of integration "panels" each having an equal number of

$\rho'$ and $\phi'$ node points. The specifics of numerical integration for RAP are discussed in [1].

## 3.5 TEST RESULTS

RAP has been tested in several ways. In each case it has performed extremely well. Thorough documentation of the test results can be found in [1, Section 8.2]. The highlights of these results are given in Table 3.5. The table gives worst case results where available.

TABLE 3.5
RAP Test Result Summary

| Geometry | $\frac{F}{D_p}$ | D(λ) | Feed | RAP Output | Output Goal |
|---|---|---|---|---|---|
| | | | | Aperture Efficiency(%) | |
| Axisymmetric | 1.0 | 20 | $\sec^2 \theta^o$ | 99.63 | (100.0) |
| | 0.5 | 40 | | 99.66 | (100.0) |
| | 0.25 | 60 | | 100.00 | (100.0) |
| | | | | Spillover Efficiency(%) | |
| Axisymmetric | 0.5 | 40 | $\cos^2 \theta^o$ | 81.96 | (81.96) |
| | | | | Side Lobe Level (dB) | |
| Axisymmetric | 1.0027 | 48 | $\beta = 17.1095$ $\cos^\beta \theta^o$ | 1st, -37.92 | (-38) |
| | | | | 2nd, -36.2 | (-36) |
| Offset | 0.46 | 100 | $\beta = 13.084$ $\cos^\beta \theta^o$ | 4th, -53.4 | (-53) |
| | | | | E-Plane SLL (dB) | |
| Offset | 0.33 | 28.64 | measured | 3rd, -34.0 | (-34.5) |
| | | | | H-Plane SLL (dB) | |
| | | | | 2nd, -31.5 | (-32) |
| | | | | 3rd, -35.5 | (-37) |
| | | | | Cross-pol lobe(dB) | |
| | | | | 1st, -22.3 | (-22) |

# 4. MULTI-ELEMENT FEED IMPLEMENTATION

As was discussed earlier, RAP employs a method of reflector analysis which includes the effects of the axial (z'-axis) component of the reflector surface currents. Nevertheless this P.O. technique is so formulated to permit evaluation of the integral in the reflector aperture. Integration is performed by a composite Gaussian-Legendre numerical quadrature where the equivalent surface currents are obtained at every node point. These equivalent currents are proportional to the incident H-field due to any number of feeds. When more than one feed (element) is present the equivalent currents are proportional to the superposition of the H-fields from each feed element. An analysis approach is presented which superimposes the H-fields from individual feed elements onto the reflector surface. The total field is used to obtain the equivalent surface currents that form the radiation integral.

The process of using superposition to find the total field from a reflector is not new [25, 19]. However, most approaches involve first computing the secondary radiation patterns of the individual elements and then superimposing these [19]. This technique is inefficient because the far-field pattern of each individual element must be obtained, often by time consuming means. However once each element pattern is obtained they can be stored, weighted, recalled, and superimposed for each field point.

Many weighting schemes can be investigated easily and efficiently because only a complex summation is needed for a superposition (i.e. further time consuming integration is not required). This process produces accurate gain and overall aperture efficiency values; however, accurate spillover efficiency is not obtained.

To summarize, there are three important advantages that the feed element superposition approach offers over that of the far-field superposition approach. First, accurate spillover values can be obtained leading to accurate gain/efficiency values. Second, the multi-element feed can be analyzed almost as fast a single feed element. And third, the elements can be located and pointed arbitrarily which is ideal for feed location and pointing optimization studies.

The coordinate component and system transformations discussed in Section 3.1 are used to define source/element relations. So, as with the reflector/feed relation, individual elements can be positioned and rotated relative to a "source" coordinate system easily. Coordinate component and coordinate system transformations can be made.

The sections to follow present the relation between the source and individual element geometries. The algorithm used for superimposing the feed elements is presented as well as the modifications to RAP.

## 4.1 GEOMETRY

A general coordinate transformation technique was developed in Section 3.1 allowing two Cartesian systems to be described in terms of one another. This transformations approach was applied to separate reflector and feed systems allowing the feed fields to be determined at the reflector surface. The approach is now extended to multiple feed element systems where each feed element is described by its own spherical geometry (Section 3.2). Essentially, a separate coordinate transformation between each feed element and a "source" system is performed. This process allows the individual feed fields to be superimposed in the source system. The total field is then used to find the surface currents.

### 4.1.1 SOURCE SYSTEM

The source system contains a total of $N_f$ separate elements forming the feed array. All individual element patterns are assumed to be identical, however this is not a fundamental restriction, only a coding convenience. When each element pattern is different, effects such as mutual coupling can be included [26]. The phase center of the complete array is assumed to be at the source system origin which is located (with respect to the reflector system origin) by the Cartesian position vector

$\bar{w}_c^o$. This is the same translation vector defined in Section 3.1. The orientation or rotation of the source system is represented by the Eulerian angles ($\alpha^\circ$, $\beta^\circ$, $\gamma^\circ$). These are also identical to those of Section 3.1.

The source system described here is the same as the feed system of the RAP algorithm. The notation is even consistent. Therefore, once the total field is obtained referenced to the source system, the RAP algorithm could then proceed. This minimizes the amount of coding (programming) changes (Section 4.3). This also permits a "closed-form" description of the feed array so that the array pattern can be integrated (Section 4.2). The array pattern integration produces the feed gain which is proportional to the absolute reflector gain [1, Section 6.2].

### 4.1.2 ELEMENT SYSTEM(S)

The source coordinate system contains the individual element systems. The element phase center is assumed to lie on the individual element system origin. All element system origins are located (with respect to the source system origin, i.e. feed array phase center) by the individual Cartesian translation vectors $\bar{w}_c^i$. The i superscript denotes the ith element system. Note that an element phase center may lie on the feed array phase center (its translation vector would be zero, i.e. ($w_x^i = w_y^i = w_z^i = 0$). The rotations of the individual element systems are

given by their Eulerian angles ($\alpha^i$, $\beta^i$, $\gamma^i$) referenced to the source system. Figure 4.1-1 shows the relation of the reflector, source and element systems.

The coordinate system transformation theory developed in Section 3.1 is used to relate the source and elements systems. Hence the same mathematical form is used to describe this relation. From equation (3.1.3-2) the ith element position vector $\bar{r}_c^i$ is found as a function of $\bar{r}_c^o$:

$$\bar{r}_c^i = [{}^iA^o]\ [\bar{r}_c^o - \bar{w}_c^i] \qquad (4.1.2\text{-}1a)$$

where the rotation matrix $[{}^iA^o]$ is evaluated using ($\alpha^i$, $\beta^i$, $\gamma^i$) in (3.1.2-5). This can be written in matrix form as

$$\begin{bmatrix} x^i \\ y^i \\ z^i \end{bmatrix} = \begin{bmatrix} A_{11} & A_{12} & A_{13} \\ A_{21} & A_{22} & A_{23} \\ A_{31} & A_{32} & A_{33} \end{bmatrix} \begin{bmatrix} x^o - w_x^i \\ y^o - w_y^i \\ z^o - w_z^i \end{bmatrix} \qquad (4.1.2\text{-}1b)$$

This relation takes a point in the source system ($x^o$, $y^o$, $z^o$) to the cooresponding equivalent point in the ith element system ($x^i$, $y^i$,$z^i$).

Once the point in the $i^{th}$ system is known ($\bar{r}^i$), the field at that point can be obtained. Using (3.1.3-4), the feed element H-field can be found in spherical components as

$$\vec{H}_s^i(\bar{r}_s^i) = \frac{e^{-jkr^i}}{4\pi\eta r^i}\ [-V(\theta^i,\phi^i)\hat{\theta} + U(\theta^i,\phi^i)\hat{\phi}] \qquad (4.1.2\text{-}2)$$

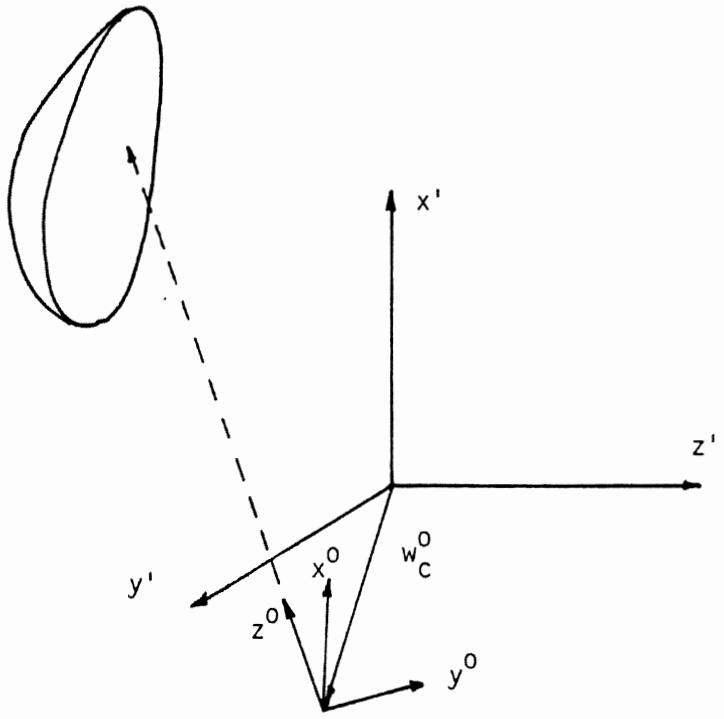


Figure 4.1-1a. Relation of the reflector and source systems

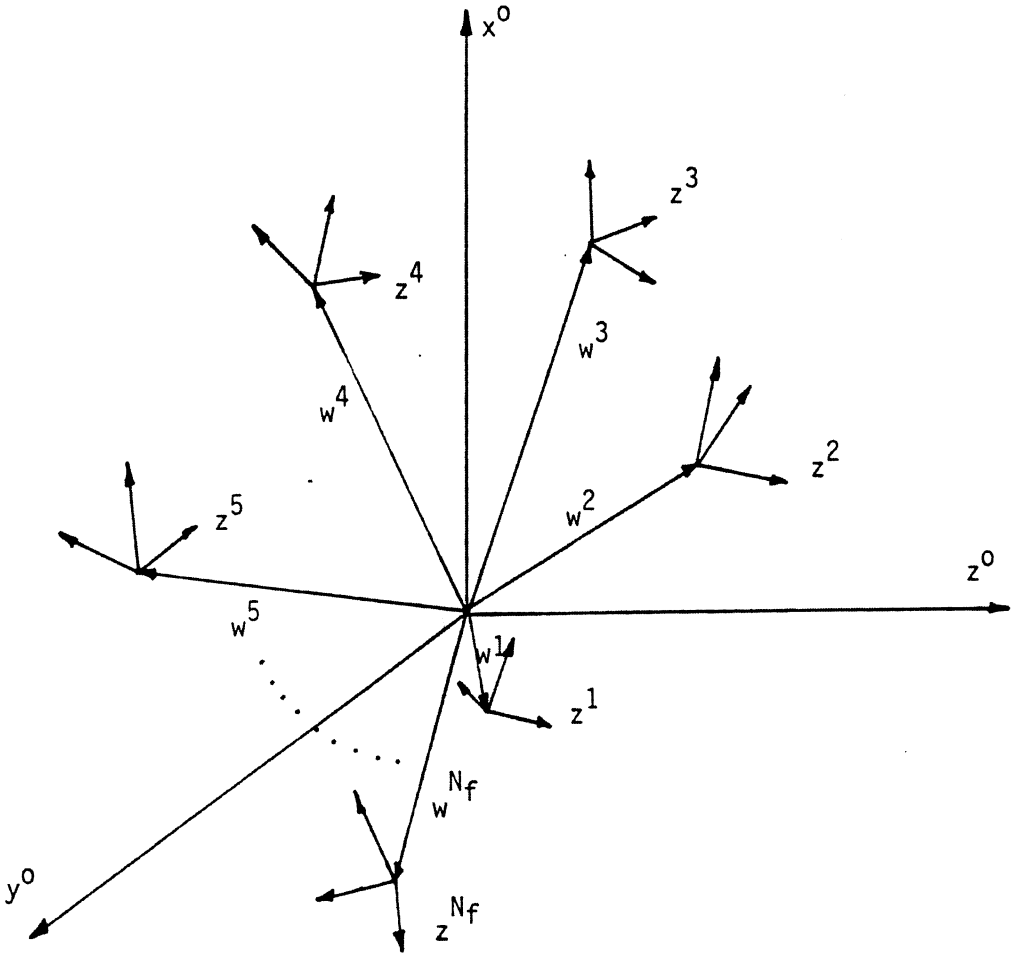


Figure 4.1-1b. Relation of the source and element systems.

The spherical components are converted to Cartesian form using $(\theta^i, \phi^i)$ in $[{}_cT_s]$ defined in (3.1.1-7). The result is obtained as

$$\vec{H}_c^i(\bar{r}^i) = [{}_cT_s]\ \vec{H}_s^i(\bar{r}^i) \qquad (4.1.2\text{-}3)$$

These Cartesian components are referenced to the $i^{th}$ system (superscript i). The fields need to be rotated to align with the source system where the superposition takes place. Equation (3.1.3-6) is used with $[{}^iA^o]$ defined in (4.1.2-1). (Note $[{}^oA^i] = [{}^iA^o]^t$ as per equation (3.1.2-8).) The identical field referenced to the source system is

$$\vec{H}_c^o = [{}^oA^i]\ \vec{H}_c^i \qquad (4.1.2\text{-}4)$$

The equations (4.1.2-2) through (4.1.2-4) may be combined into one equation giving a form similar to (2.3.1-18) as follows:

$$\vec{H}_c^{o}(\bar{r}_s^{i}) = \begin{bmatrix} H_x^o \\ H_y^o \\ H_z^o \end{bmatrix} = \begin{bmatrix} A_{11} & A_{21} & A_{31} \\ A_{12} & A_{22} & A_{32} \\ A_{13} & A_{23} & A_{33} \end{bmatrix}$$

$$\begin{bmatrix} \sin\theta^i \cos\phi^i & \cos\theta^i \cos\phi^i & -\sin\phi^i \\ \sin\theta^i \sin\phi^i & \cos\theta^i \sin\phi^i & \cos\phi^i \\ \cos\theta^i & -\sin\theta^i & 0 \end{bmatrix}$$

$$\begin{bmatrix} 0 \\ -V(\theta^i, \phi^i) \\ U(\theta^i, \phi^i) \end{bmatrix} \frac{e^{-jkr^i}}{4\pi\eta r^i} \qquad (4.1.2\text{-}5)$$

Note the rotation matrix $[{}^{o}A^{i}]$ above is defined by the Eulerian angles $(\alpha^i, \beta^i, \gamma^i)$. These angles are referenced to the source system.

## 4.2 SUPERPOSITION

The individual feed element H-fields $\vec{H}_c^i$ are superimposed in the source system. Starting at a point in the source system $\vec{r}_c^{o}$ (where the superposition takes place), the corresponding points in all $N_f$ element systems can be found ($\bar{r}_c^i$) using (4.1.2-1). The Cartesian position vector for the $i^{th}$ system can be converted to its spherical counterpart ($\bar{r}_s^i$) using Table 3.1-1. And, the field at the point $\bar{r}_s^i$ can be found using

(4.1.2-5) resulting in $\vec{H}^o_c(\bar{r}^i_s)$. This is the field due to the $i^{th}$ feed element referenced to the source system in Cartesian components.

The total field at the source system point $\bar{r}^o$ is the superposition of all $N_f$ element fields. This is

$$\vec{H}^o_c(\bar{r}^o) = \sum_{i=1}^{N_f} \vec{H}^o_c(\bar{r}^i_s) \qquad (4.2\text{-}1)$$

where $\vec{H}^o_c(\bar{r}^i_s)$ is defined in (4.1.2-5).

A complex weighting (excitation) coefficient for each element is easily included at this point. This dimensionless coefficient is written for the $i^{th}$ element as $I_i$. It consists of a magnitude and phase weight. Equation (4.2-1) is rewritten using element weightings $I_i$ as

$$\vec{H}^o_c(\bar{r}^o) = \sum_{i=1}^{N_f} I_i \, \vec{H}^o_c(\bar{r}^i_s) \qquad (4.2\text{-}2)$$

The total field summed in this fashion can be used to find the equivalent surface currents due to all $N_f$ feed elements with weighting coefficients $I_i$. Also, when the field is superimposed at great distances from the feed array ($|\bar{r}^o_c|$ >> effective array diameter) a far-field array pattern can be written using array theory [18]; however, most formulations can not include arbitrary element patterns, locations and orientations (such as in [19]). The far-field pattern of the array can be written in spherical components as

$$\vec{H}^o_s(\bar{r}^o_s) = [{}_sT_c] \, \vec{H}^o_c(\bar{r}^o) \qquad (4.2\text{-}3)$$

where $[{}_sT_c]$ is defined from (3.1.1-4) using $(\theta^o, \phi^o)$. The component form (4.2-3) is

$$\vec{H}_s^o(\bar{r}_s^o) = \begin{Bmatrix} H_r^o \\ H_\theta^o \\ H_\phi^o \end{Bmatrix} \qquad (4.2\text{-}4)$$

where the r-component is assumed to be zero (when truly in the far-field). Equation (4.2-4) becomes

$$\vec{H}_s^o(\bar{r}_s^o) = [-V_T(\theta^o,\phi^o)\hat{\theta} + U_T(\theta,\phi^o)\hat{\phi}] \frac{e^{-jkr^o}}{4\pi\eta r^o} \qquad (4.2\text{-}5)$$

where the spherical spreading loss and spherical phase front are shown explicitly in the last factor. Note that (4.2-5) is in a form very similar to (3.2-3) allowing the total E-field to be written as

$$\vec{E}_s^o(\bar{r}_s^o) = [U_T(\theta^o, \phi^o)\hat{\theta} + V_T(\theta^o, \phi^o)\hat{\phi}] \frac{e^{-jkr^o}}{4\pi r^o} \qquad (4.2\text{-}6)$$

The $U_T$ and $V_T$ represent the far-field radiation patterns of the total feed array field.

It was shown in [1] that given the far-field radiation patterns of the feed array the power radiated by the array can be obtained. Much effort has been directed toward efficiently finding the power radiated [27]. However, most techniques required restricted feed geometries such as planar arrays. We obtained a more general formulation.

The power radiated from the feed [1] is proportional to the integral given below

$$P = \int_0^{2\pi}\int_0^{\pi} \{|U_T(\theta^o, \phi^o)|^2 + |V_T(\theta^o, \phi^o)|^2\} \sin\theta^o \, d\theta^o \, d\phi^o \qquad (4.2\text{-}7)$$

where $U_T$ and $V_T$ are defined in (4.2-6). RAP employed a back-to-back adaptive Simpson's Rule which worked well for smooth, slowly varying feed patterns. However the array pattern can often be rapidly varying. We found that a "brute-force" back-to-back trapezoidal rule offers consistent accuracy in evaluating (4.2-7). The drawback to trapezoidal rule integration is that it is time consuming; however, feed array symmetry was exploited to shorten run times.

## 4.3 RAP MODIFICATIONS

The theory developed in sections 4.1 and 4.2 was implemented by modifying the Reflector Antenna Program (RAP). The new multiple feed reflector analysis program was given the acronym MFRAP (Multiple Feed Reflector Antenna Program). Note that the multiple feed algorithm was developed with RAP in mind; consequently, minimal changes in RAP were required. Essentially, only the parts in RAP pertaining to the feed description were changed. These changes will be discussed.

The summary steps of subsection 2.3.2 gave a brief description of the RAP algorithm. More specifically, steps 2.3.2-1 through 5 pertain to the reflector/feed coordinate system relations. Table 4.3-1 gives an alternate representation of these summary steps, describing the process more visually. The arrows in Table 4.3-1 show the direction of algorithm flow ending at the surface current ($\bar{J}$) calculation.

A similar MFRAP representation is given in Table 4.3-2 where the reflector/source/element coordinate system relation algorithm is shown. It is easy to see where the RAP and MFRAP algorithms differ. Therefore, only the steps in which MFRAP is different from RAP are presented in the summary.

A step-by-step summary of the MFRAP algorithm is given next. The RAP and MFRAP algorithms are so similar that only the differing steps are presented. Essentially, RAP steps 4) and 5) of subsection 2.3.2 are replaced forming the MFRAP approach.

1. After the Cartesian components of the reflector point relative to the source system $\bar{r}_c^o$ have been found (4.3-1) (step 2.3.2-3), the corresponding point $(x^i, y^i, z^i)$ is determined by (4.1.2-1) for the $i^{th}$ system. (4.3-1)

2. The Cartesian point $(x^i, y^i, z^i)$ is converted to its spherical representation $(r^i, \theta^i, \phi^i)$ giving $(\bar{r}_s^i)$. (4.3-2)

Table 4.3-1

RAP Coordinate System Transformation Summary*

| Coordinate System (Superscript) | Component Representation (Subscript) SPHERICALS(s) | CARTESIAN(c) | CYLINDRICAL($\bar{c}$) |
|---|---|---|---|
| Reflector (primed) | | $\bar{r}'_c$ | $\bar{r}'_{\bar{c}}$ |
| Feed or Source (super o) | $\bar{r}^o_s$ | $\bar{r}^o_c$ | |
| Feed or Source (super o) | $\bar{H}^o_s(\bar{r}^o_s)$ | $\bar{H}^o_c(\bar{r}^o_s)$ | |
| Reflector (prime) | | $\bar{H}'_c$ | |
| Reflector (prime) | | $\bar{J}'_c$ | |

(2.3.2-1) $\bar{r}'_{\bar{c}} \rightarrow \bar{r}'_c$

(2.3.2-3) $\bar{r}'_c \rightarrow \bar{r}^o_c$

(2.3.2-4) $\bar{r}^o_c \rightarrow \bar{r}^o_s$

(2.3.2-4) $\bar{r}^o_s \rightarrow \bar{H}^o_s(\bar{r}^o_s)$

(2.3.2-5) $\bar{H}^o_s(\bar{r}^o_s) \rightarrow \bar{H}^o_c(\bar{r}^o_s)$

(2.3.2-5) $\bar{H}^o_c(\bar{r}^o_s) \rightarrow \bar{H}'_c$

$\bar{H}'_c \rightarrow \bar{J}'_c$

Repeat for all Current Locations

*The numbers in parenthesis represent the summary steps of subsection 2.3.2.

3. The point $\bar{r}_s^i$ is used in (4.1.2-5) to obtain the H-field due to the $i^{th}$ element relative to the source system $\vec{H}_c^o(\bar{r}^i)$ (4.3-3)

4. These Cartesian components are weighted and stored in a running sum where after all fields have been superimposed form the total field $\vec{H}_c^o(\bar{r}^o)$. This is equation (4.2-2) (4.3-4)

5. The total field is rotated by (3.1.3-6) to align with the reflector system giving $\vec{H}_c'$. This is used in (2.3.2-7) where the RAP algorithm continues. (4.3-5)

Table 4.3-2

MFRAP Coordinate System Transformation Summary*

| Coordinate System (Superscript) | Component Representation (Subscript) SPHERICAL(s) | CARTESIAN(c) | CYLINDRICAL($\bar{c}$) |
|---|---|---|---|
| Reflector (prime) | | $\bar{r}_c'$ | $\bar{r}_{\bar{c}}'$ |
| Source (super o) | | $\bar{r}_c^o$ | |
| Individual Element (super i) | $\bar{r}_s^i$ | $\bar{r}_c^i$ | |
| Individual Element (super i) | $\bar{R}_s^i(\bar{r}_s^i)$ | $\bar{R}_c^i(\bar{r}^i)$ | |
| Source (super o) | | $\bar{R}_c^o(\bar{r}^i)$ | |
| Source (super o) | | $\bar{R}_c^o(\bar{r}^o)$ | |
| Reflector (prime) | | $\bar{R}_c'$ | |
| Reflector (prime) | | $\bar{J}_c'$ | |

(2.3.2-1) connects $\bar{r}_{\bar{c}}'$ to $\bar{r}_c'$; (2.3.2-3) connects $\bar{r}_c'$ to $\bar{r}_c^o$; (4.3-1) connects $\bar{r}_c^o$ to $\bar{r}_c^i$; (4.3-2) connects $\bar{r}_c^i$ to $\bar{r}_s^i$; (4.3-3) connects $\bar{r}_s^i$ to $\bar{R}_s^i(\bar{r}_s^i)$; (4.3-4) connects $\bar{R}_s^i(\bar{r}_s^i)$ to $\bar{R}_c^i(\bar{r}^i)$; (4.3-4) connects $\bar{R}_c^i(\bar{r}^i)$ to $\bar{R}_c^o(\bar{r}^i)$; (4.3-4) connects $\bar{R}_c^o(\bar{r}^i)$ to $\bar{R}_c^o(\bar{r}^o)$; (4.4-5) connects $\bar{R}_c^o(\bar{r}^o)$ to $\bar{R}_c'$; $\bar{R}_c'$ to $\bar{J}_c'$. Repeat for all $N_f$ elements. Repeat for all current locations.

*The numbers in parenthesis represent the summary steps of subsections 2.3.4 and 4.3.

# 5. MULTIPLE FEED REFLECTOR ANTENNA PROGRAM - MFRAP

The previous chapters of this report involved the development of the theory suited for reflector antenna analysis. In particular, theory for a multiple feed element reflector was discussed. This chapter contains information on program flow, subroutine description and program execution for the Fortran 77 code MFRAP. The chapter is written to help other users who might want to implement or modify MFRAP for their own purposes. Example inputs and outputs are examined with particular interest directed towards element orientations (rotating by Eulerian angles).

To show the accuracy of this technique, results from MFRAP are compared to those of P. T. Lam and S. W. Lee [19, 28]. In all cases, MFRAP performed well.

To show the usefulness of MFRAP, a short investigation was made on the effects of element pointing on reflector performance. The study gives a good representation of how MFRAP could be used to investigate an aspect of multiple feed element reflectors. The ability to arbitrarily point, position and excite the feed elements allows many different scenarios to be examined.

## 5.1 OVERVIEW OF MFRAP

As was discussed in Chapter 4, MFRAP is based on the single feed reflector analysis program RAP (Reflector Antenna Program). The theory and coding for RAP was developed with subsequent changes in mind to facilitate coding modifications. Consequently only the RAP feed element algorithm required modification to create MFRAP. This section discusses the major modifications to the source code RAP. The reader is referred to [1] for complete documentation on and usage of RAP. The Reflector Antenna Program Organization is show in Figure 5.1-1. It may be compared to the MFRAP organization chart in Figure 5.1-2. It is noted that only slight modifications were necessary.

The block diagram of Figure 5.1-2 shows that MFRAP consists of four major sections, each section performing a major function; those are discussed in the remaining subsection of this section.

The subroutines which are new or modified from RAP are discussed here. First, the additional values (arguments) passed in common blocks are outlined briefly in Tables 5.1-1 through 5.1-5. Only modified common blocks are discussed.

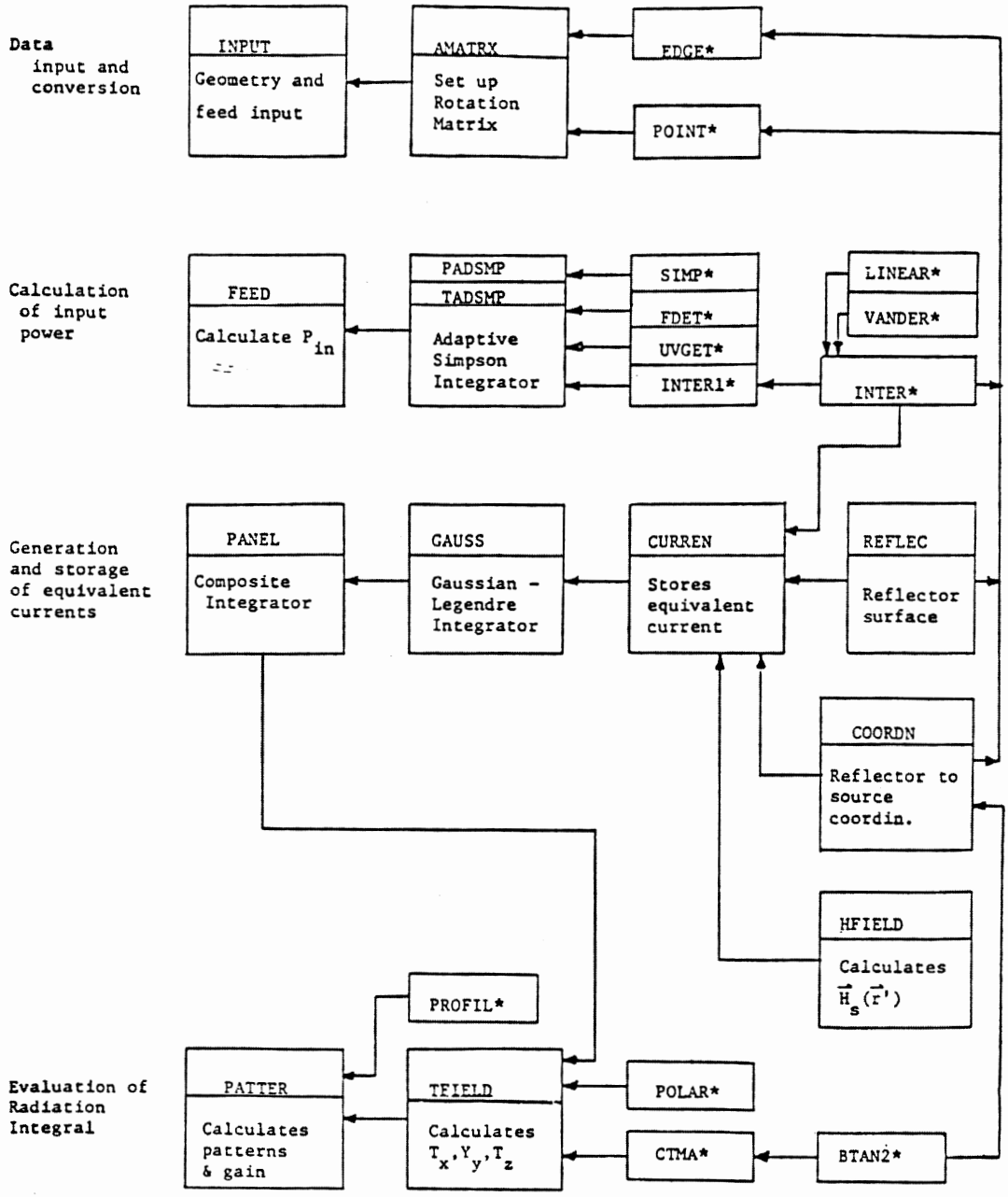


Figure 5.1-1. The Reflector Antenna Program (RAP) Organization.
*Utility Subprograms

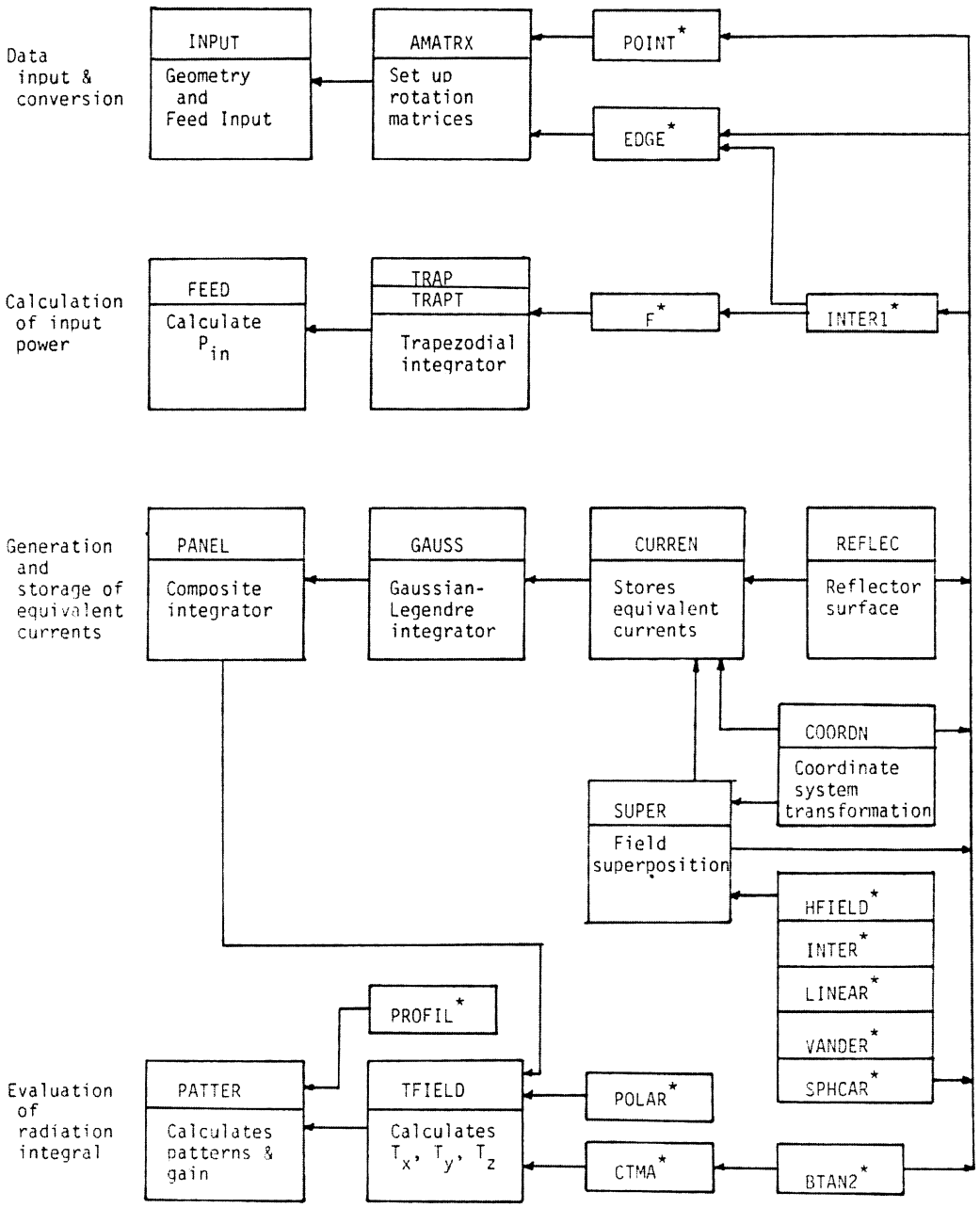


Figure 5.1-2 The Multiple Feed Reflector Antenna Program (MFRAP) Organization. *Utilty Subprograms

## Table 5.1-1

Common Block /BLOC1/

| Argument | | Description |
|---|---|---|
| QQE | ; | Value of $q_E$ input when LREAD = F. Used to calculate E-plane feed pattern with $\cos^{q} \theta°$. |
| QQH | ; | Same as $q_E$ above except for H-plane of feed pattern |

## Table 5.1-2

Common Block /BLOC2/

| Argument | | Description |
|---|---|---|
| RSSAVE | ; | Stores $\lvert\bar{r}°\rvert$ for calculating total H-field at the point $\bar{r}°$. |

Table 5.1-3

Common Block /BLOC3/

| Argument | | Description |
|---|---|---|
| SPHER(3) | ; | Array for storing any spherical position vector (r, θ, ϕ). |
| CART(3) | ; | Array for storing any Cartesian position vector (x, y, z). |

Table 5.1-4

Common Block /BLOC4/

| Argument | | Description |
|---|---|---|
| HXT<br>HYT<br>HZT | ;<br>;<br>; | Cartesian components of total (superimposed) H-field. |
| WX (0 : NF)<br>WY (0 : NF)<br>WZ (0 : NF) | ;<br>;<br>; | Arrays for storing the Cartesian translation vectors $W^{o}$ through $W^{N_f}$ |

Table 5.1-5

Common Block /BLOC12/

| Argument | | Description |
|---|---|---|
| WMAG<br>WPHA | ;<br>; | Magnitude and phase weights for excitation coefficients |
| NFEED | ; | Number of total feed elements |
| NPOINT | ; | Number of feed elements to point. Used when automatic pointing option is chosen. (LPOINT = T) |

### 5.1.1 DATA INPUT AN CONVERSION

The first section consists of four subroutines that control input/ouput, reflector geometry and internal storage organization. The controlling subroutine INPUT is used to input and convert all geometry and feed data from the input files and echo this (and calculated) data to the output file. The input file format is discussed in Section 5.3. The modifications to the RAP version are slight. Essentially, only the ability to input and store the multiple feed parameters (such as; translation vectors, Eulerian angles, element weights, etc.) was added.

The subroutines AMATRX, POINT, and EDGE were also modified. Their functions are identical to those of RAP. However, modifications were needed to allow the routines to function for any feed element (the integer argument IF is used to denote the element number). For example, AMATRX is now called with the additional argument IF. The routine uses the Eulerian angles ($\alpha^i$, $\beta^i$, $\gamma^i$) to determine the rotation matrix $[{}^iA^o]$ of equation (3.1.2-5). The changes to subroutines EDGE and POINT are similar.

### 5.1.2 CALCULATION OF INPUT POWER

The second section of MFRAP evaluates the integral in equation (4.2-7), determines the power radiated by the feed array, and calculates

the feed array gain. This section was changed from a two-dimensional adaptive Simpson integration to a "brute-force" back-to-back trapezoidal rule approach. It was found that the adaptive algorithm creates excessive run times (often without convergence) for feed arrays with element spacings greater than 1 $\lambda$. The algorithm was struggling to integrate the grating lobes produced by such spacings [18].

This portion of code was verified by comparing feed array gain to published work arrays (with no reflection involved). Table 5.1-6 shows good agreement between the MFRAP feed gain calculation and those presented in this literature [27, 29, 18]. Results indicate that integration with one degree samples gives adequate results.

An important change between RAP and MFRAP is the subroutine INTER1. The modified subroutine calculates the total field at the point $\bar{r}_s^o$ due to all feed elements. The routine accounts for the spherical phase front and spherical spreading loss terms given in equation (4.2-5). The remaining field quantities are returned in the form of spherical components (HRT, HTT, HPT). Note that the $\hat{r}$ component is zero when the point $\bar{r}_s^o$ is in the far-field. This array pattern is integrated for the resulting components represent the far-field array pattern. This array pattern is integrated for the power radiated calculation. Various array patterns from MFRAP were checked with theoretical results [27]. In all cases, MFRAP performed well.

## Table 5.1-6

Examples of Feed Array Gain Calculation

| # of Elements | Spacing | Array Structure | Q* | MFRAP Directivity | Theoretical Directivity |
|---|---|---|---|---|---|
| 1 | - | singlet | $q_E = 0$<br>$q_H = 0$ | 2.015 | 2.0 |
| 9 | 0.5 λ | linear | $q_E = 0$<br>$q_H = 0$ | 18.094 | 18.0 |
| 9 | 1.4 λ | square (3 x 3) | $q_E = 2.6$<br>$q_H = 1.9$ | 19.99 dB | 20 dB |
| 7 | 0.8 λ | cluster** (equal weights) | $q_E = 2.6$<br>$q_H = 1.9$ | 18.02 dB | 18 dB |
| 7 | 1.8 λ | cluster** (equal weights) | $q_E = 0$<br>$q_H = 0$ | 11.72 dB | 11.6 dB |
| 7 | 1.8 λ | cluster** (equal weights) | $q_E = 8.7$<br>$q_H = 5.25$ | 22.99dB | 22.94 dB |
| 7 | 1.8 λ | cluster** (equal weights) | $q_E = 8.7$<br>$q_H = 5.25$ | 21.02 dB | 20.98 dB |

* Q represents E- and H- plane q used in $\cos^q \theta$ feed element pattern.

** Cluster indicates triangular lattice type of Section 5.2.

### 5.1.3 EQUIVALENT CURRENT GENERATION AND STORAGE

The third section of MFRAP is so configured to allow rapid evaluation of the large radiation integral without recalculation of the entire integrand. Figures 5.1-1 and 5.1-2 indicate that subroutines SUPER and SPHCAR were added to the MFRAP algorithm. The remaining program flow is identical to RAP. These new and important routines are discussed here.

The subroutine SPHCAR performs a very simple function yet is quite useful. This routine converts a position vector from spherical to Cartesian components when the integer argument IFLAG is greater than zero. The routine will also convert from Cartesian to spherical components when IFLAG is less than zero. The routine is used often.

The subroutine SUPER performs the superposition function given by equations (4.1.2-1), (4.1.2-5), and (4.2-2). The algorithm uses the Cartesian point $\bar{r}_c^o$ stored in the array COORD as input. The routine calculates, for each feed element, the field at point $\bar{r}_c^o$. The superposition function is performed by a simultaneous running-sum operation. The routine produces the total field in Cartesian components (HXT, HYT, HZT) as output. These field values are used in (3.3-7) to give the equivalent surface currents of the radiation integral (3.4-1).

The subroutines COORDN, INTER and HFIELD were slightly modified. Routine COORDN now accepts a Cartesian position vector stored in the array COORD and converts it to its corresponding Cartesian representation of another system. Essentially equation (4.1.2-1) is used. The new Cartesian vector is stored in the array CART. The subroutines INTER and HFIELD were expanded to accept and calculate the fields for the $i^{th}$ system (denoted by the integer argument IF).

### 5.1.4 EVALUATION OF RADIATION INTEGRAL

There are no changes between the MFRAP and RAP versions.

## 5.2 MFRAP GEOMETRY

The complex geometry of MFRAP is many "layers" deep. There are many systems related to one another. To simplify matters, these system relations will be discussed in the following order: far-field/reflector, reflector/source and source/element. Figure 5.2-1 shows the offset reflector geometry with some important parameters defined. The projected reflector perimeter is defined in the aperture (x', y') plane. The blockage region is given by the ellipse with axises $C_r$ and $D_r$. Note for offset geometries the blockage region will probably be zero, but it is

given here for completeness. To reduce the abstract nature of the MFRAP geometry, the following discussion illustrates a typical Reflector/Source/Element situation.

A specific reflector/source geometry is given in Figure 5.2-2 as an example. This is the geometry used to reproduce the results of Shung-Wu Lee and P. R. Lam [19]. The reflector and source systems are related by the translation vector $\bar{w}_c^o$ and Eulerian angles ($\alpha^o$, $\beta^o$, $\gamma^o$). The correct choice of the Eulerian angles is important. For example, if $\gamma^o$ was chosen to be -90° the $x^o$-axis would be pointing down instead of up. This difference could be a drastic change from the desired geometry. Therefore, the user must be sure of the geometric input and be aware that an input mistake could drastically change the reflector/source geometry. The reasons for this should become clearer as the discussion continues.

The source/element systems are related by the translation vectors $\bar{w}_c^i$ and Eulerian angles ($\alpha^i$, $\beta^i$, $\gamma^i$). These positions and orientations of the elements form the feed array. So, it should be noted that the feed array, as a whole, is rotated with the Eulerian angles ($\alpha^o$, $\beta^o$, $\gamma^o$). Therefore, and Eulerian angle sign change, such as in the example given in the previous paragraph could change how the feed array illuminates the reflector.

The multiple beam reflector antenna feed array usually consists of numerous (identical) feed elements arranged in a triangular lattice type structure. The array is often planar with all elements pointing in the same direction. The array lattice is given in Figure 5.2-3 where the

element spacing is given by the distance d [19]. The dots 1 through 19 represent the element phase center locations ($\bar{w}_c^i$). The central element (number 1) is located at the feed array phase center (source system origin). This phase center is located with respect to the reflector system origin by the translation vector $\bar{w}_c^o$. The entire array is easily moved (to scan the reflector pattern main beam) by one translation vector.

The pointing of the feed elements are given by the Eulerian angles ($\alpha^i$, $\beta^i$, $\gamma^i$). These are defined with respect to the source system. Therfore with $\alpha^i = \beta^i = \gamma^i = 0$ all elements point in the $z^o$ direction. This is the most commonly used feed array orientation. Other element pointings are possible. Some of these pointings are investigated in Section 5.4. But in the next section inputs and outputs of MFRAP are presented.

## 5.3 USERS GUIDE TO MFRAP

The close similarities between RAP and MFRAP allowed minimal changes between input file formats. In fact, MFRAP and RAP use the same logical file numbers (LFN): 20, 21 and 22. Only LFN 20 differs between the two codes. The input file format for LFN 20 is discussed.

LFN 20 contains the input for reflector, source and element geometries. This file controls program flow and determines how to read the files assigned to LFN 21 and 22. All input files are unformatted,

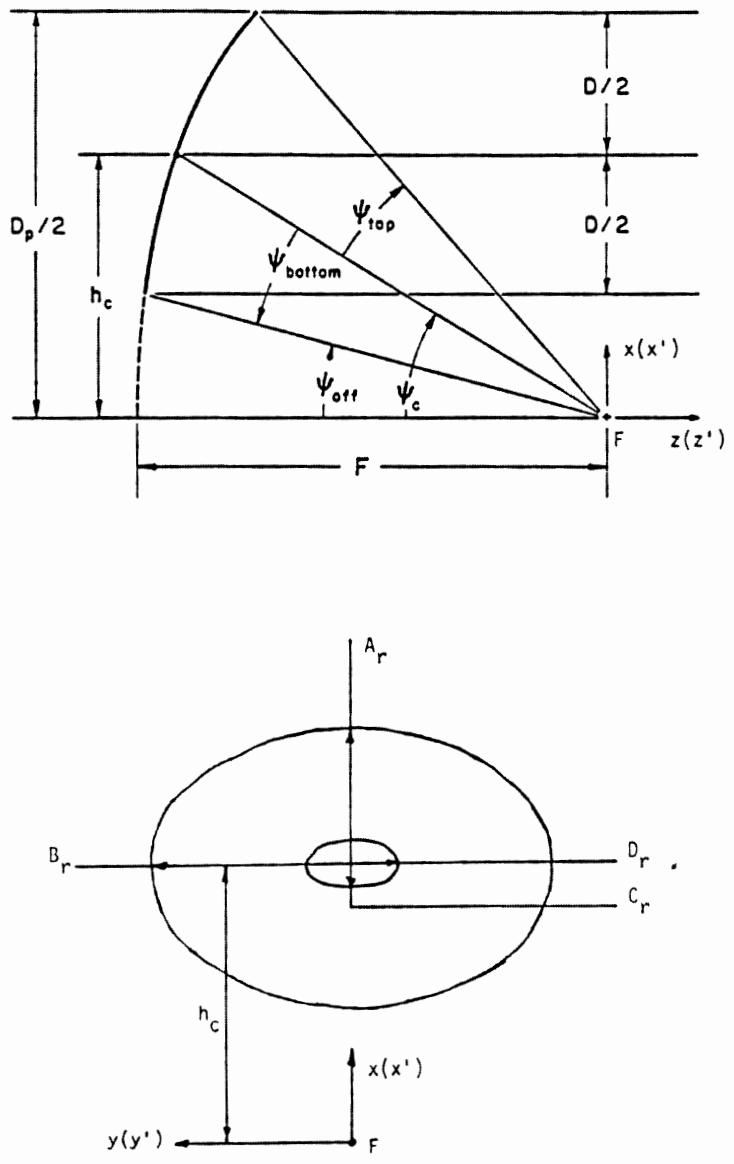


Figure 5.2-1 Offset Reflector Geometry

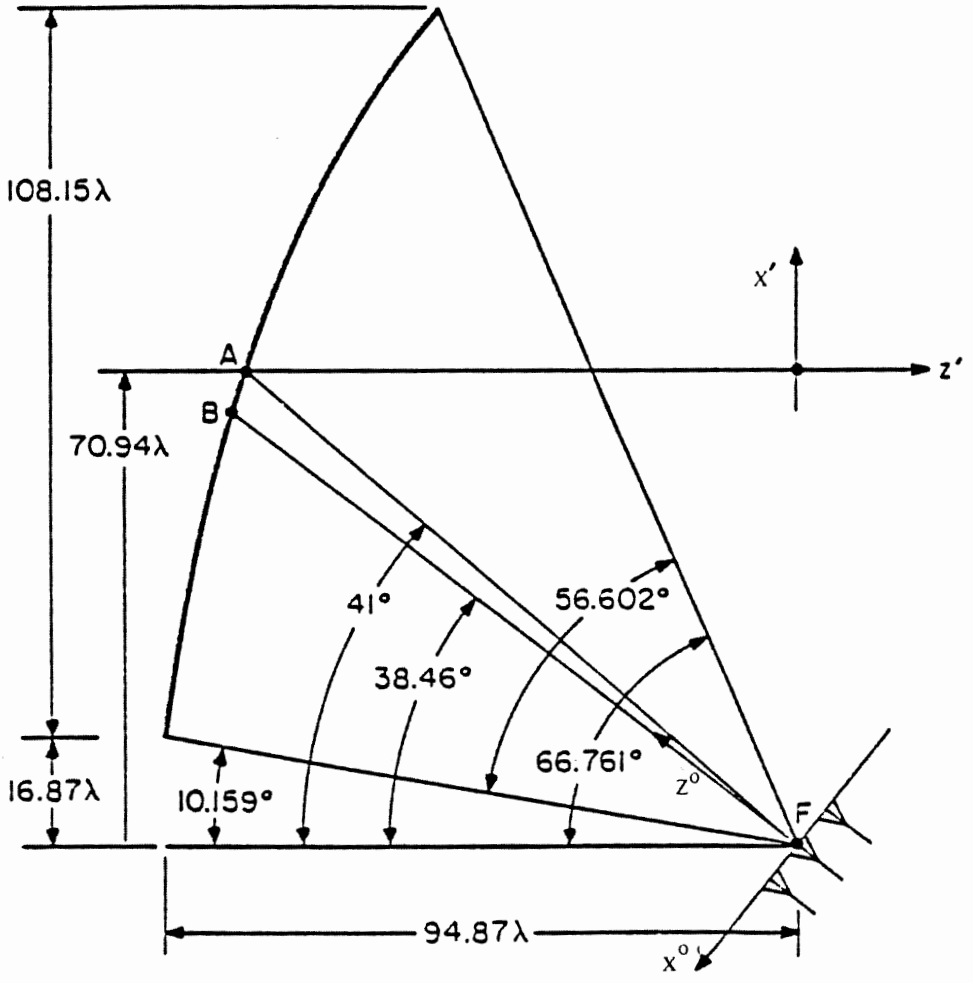


Figure 5.2-2 Specific reflector/source geometry. From [19]

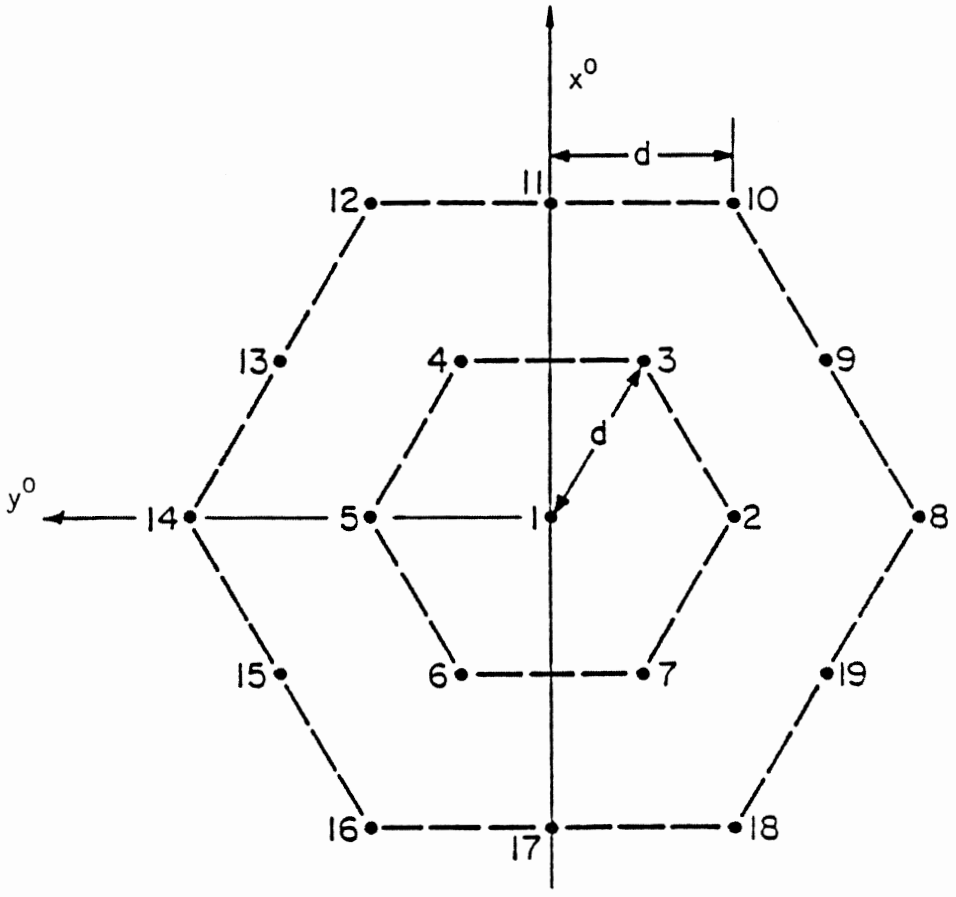


Figure 5.2-3 Array lattice structure. From [19]

hence only spaces (or commas) are needed to separate the input variables. The general form of the LFN 20 input file is given next. The reader is referred to [1] for LFN 21 and 22 input file formats.

LFN 20

```
LINPOL, LVERT, LDB, LSYM, LPLOT, LREAD, LWRITE, LPOINT, LSPHER
NFEED, NPOINT, NPPLOT
ALPHA(0), BETA(0), GAMMA (0), WX(0), WY(0), WZ(0)
  .        .        .        .     .     .
  .        .        .        .     .     .
  .        .        .        .     .     .
  .        .        .        .     .     .
  .        .        .        .     .     .
ALPHA(NFEED), BETA(NFEED), GAMMA(NFEED), WX(NFEED), WY(NFEED), WZ(NFEED)


WMAG(1),  WPHA(1)
   .         .
   .         .
WMAG(NFEED), WPHA(NFEED)

*(LREAD option)
ARAD, BRAD, CRAD, DRAD
```

FOCAL, OFFSET

*(ICONV option)

NPANEL, NORDER

THETAB, THETAE, THETAI

PHIB, PHIE, PHII

MTRAPT, MTRAP, BEGIN, END, ENDT

The asterisks above indicate options which might modify the input file. These option blocks are discussed below and should be inserted into their respective locations above. The input variables for LFN 20 are listed in Table 5.3.

## Table 5.3

INPUT VARIABLE DESCRIPTION FOR LFN 20

| ARGUMENT | TYPE* | DESCRIPTION |
|---|---|---|
| LINPOL | L | linear polarization flag:<br>True, linear polarized system<br>False, circular polarized system |
| LVERT | L | polarization flag:<br>(If LINPOL is True)<br>True, vertical polarized reflector<br>False, horizontal polarized reflector<br>(if LINPOL is False)<br>True, right hand circularly polarized feed<br>False, left hand circularly polarized feed |
| LDB | L | feed decibel flag:<br>True, feed magnitude in dB<br>False, feed magnitude in field |
| LSYM | L | feed symmetry flag:<br>controls LSYM option block |
| LPLOT | L | plotting option:<br>True, feed and far-field pattern plotted<br>False, no plot generated |
| LREAD | L | feed pattern input flag:<br>controls LREAD option block |
| LWRITE | L | output control flag:<br>True, all output written<br>False, limited output written |
| LPOINT | L | automatic pointing option:<br>True, feed tilted to dish center<br>False, input ALPHA, BETA, GAMMA used. |

| | | | |
|---|---|---|---|
| LSPHER | L | | spherical reflector option:<br>True, spherical reflector surface<br>False, parabolic reflector surface |
| NFEED | I | | number of feed elements |
| NPOINT | I | | number of feed systems to automatically point towards geometric dish center. (LPOINT must be True) |
| NPPLOT | I | | number of feed pattern points to plot |
| ALPHA(0) to (NFEED)<br>BETA(0) to (NFEED)<br>GAMMA(0) to (NFEED) | R<br>R<br>R | | source and element system Eulerian angles (degrees) |
| WX(0) to (NFEED)<br>WY(0) to (NFEED)<br>WZ(0) to (NFEED) | R<br>R<br>R | | source and element translation vectors (wavelengths, inches or meters) |
| WMAG(1) to (NFEED) | | R | excitation coefficients for feed elements, magnitude (field) phase (degrees) |
| (LREAD option) | | | |
| NTHETS | | I | number of theta points per phi cut |
| TSINC | | R | size of angle between adjacent theta points (degrees |
| NPHIS | | I | number of phi cuts to input |
| PSINC | | R | size of angle between adjacent phi cuts = 90° |
| (LSYM option) | | | |
| 1<br>2 | | I | controlling phi cut number which is symmetric to others |
| NSCUTS | | | |
| NSCUTS | | I | the number of phi cuts which are symmetric to controlling number |
| INDIV(1) | | I | phi cut number symmetric to |

| | | |
|---|---|---|
| INDIV(2) | | controlling number |
| . | | |
| . | | |
| INDIV(NSCUTS) | | |
| QQE | R | $q_E$ used in $\cos^{qE}\theta$ E-plane feed pattern |
| QQH | R | $q_H$ used in $\cos^{qH}\theta$ H-plane feed pattern |
| ARAD | R | x-dimension radius of aperture |
| BRAD | R | y-dimension radius of aperture |
| CRAD | R | x-dimension radius of blockage area |
| DRAD | R | y-dimension radius of blockage area (wavelengths, inches or meters) |
| FOCAL | R | focal length of parabolic reflector with diameter $D_p$ (LSPHER=F) or radius of spherical reflector (LSPHER=T) (wavelengths, inches, or meters) |
| OFFSET | R | offset height ($h_c$) of aperture |
| (ICONV option) | | |
| ICONV | I | 0-lengths in wavelengths<br>1-lengths in inches<br>2-lengths in meters |
| FREQ | R | frequency of radiation (GHz) |
| NPANEL | I | number of 'panels' reflector aperture is integrated over |
| NORDER | I | order of Gaussian quadrature (the number of integration points in the aperture is NPANEL x NORDER x NORDER) |
| THETAB | R | far-field beginning angle (degrees) |
| THETAE | | far-field ending angle (degrees) |
| THETAI | | far-field increment angle (degrees) |

| | | |
|---|---|---|
| PHIB | R | far-field beginning angle )degrees |
| PHIE | | far-field ending angle (degrees) |
| PHII | | far-field increment angle (degrees) |
| MTRAPT | I | number of points used in trapezoidal feed patterns integration in $\theta^\circ$ |
| MTRAP | I | number of points used in feed pattern integration in $\phi^\circ$ |
| BEGIN | R | beginning and ending feed pattern integration $\theta^\circ$ variables (degrees) |
| END | R | |
| ENDT | R | ending feed pattern integration $\theta^\circ$ variable. (0.0 is assumed as beginning $\theta^\circ$ variable). (degrees) |

*Fortran type: L - logical
I - integer
R - real

The LREAD option controls the reading of the feed pattern in LFN 20. If LREAD
is true then insert the following at location (LREAD option) above:

```
NTHETS, TSINC
NPHIS, PSINC
*(LSYM option)
```

If LREAD is false, then input: QQE, QQH

The LSYM option (above) is used to generate additional phi-cuts with the use of symmetry. If LSYM in line 1 of LFN 20 is true, input the following at location (LSYM option) above:

```
1, NSCUTS, INDIV(1), INDIV(2), .... INDIV(NSCUTS)

2, ............
.
.
.
NPHIS ..........
```

If LSYM is false, then input nothing

The ICONV option specifies the unit of length used to input every length dimension (i.e., ARAD, BRAD FOCAL, etc.). In the location of the (ICONV option) above, ICONV is input and

If ICONV = 0, units are wavelengths and nothing else is input.

If ICONV = 1, units are inches and frequency is gigahertz is input on the following line.

If ICONV = 2, unit are meters and frequency in gigahertz is input on the following line.

## 5.3.1 INPUT AND OUTPUT EXAMPLES

In order to illustrate how MFRAP is used, input and output examples are given in this subsection. The form of the required input file (LFN 20) is included with each example.

Example 1: Offset parabolic reflector with single element feed (singlet).

The reflector is vertically polarized with an approximate edge taper of -10 dB. The feed pattern is given by the symmetric analytic function $\cos^q \theta°$. The reflector geometry is given in Figure 5.3.1-1 where the feed is scanned 5.53λ to produce a 5 BW scan. Blockage is neglected.

- Input (LFN 20):

```
T, T, F, F, T, F, T, F, F
1, 0, 0
90.0, 141.54, 90.0, -4.33, 0.0, -3.44
0.0, 0.0, 0.0, 0.0, 0.0, 0.0
1.0, 0.0
9.0442   9.0442
54.075, 54.075, 0.0, 0.0
94.87, 70.94
0
4, 20
1.0, 5.0, 0.05
0.0, 0.0, 90.0
```

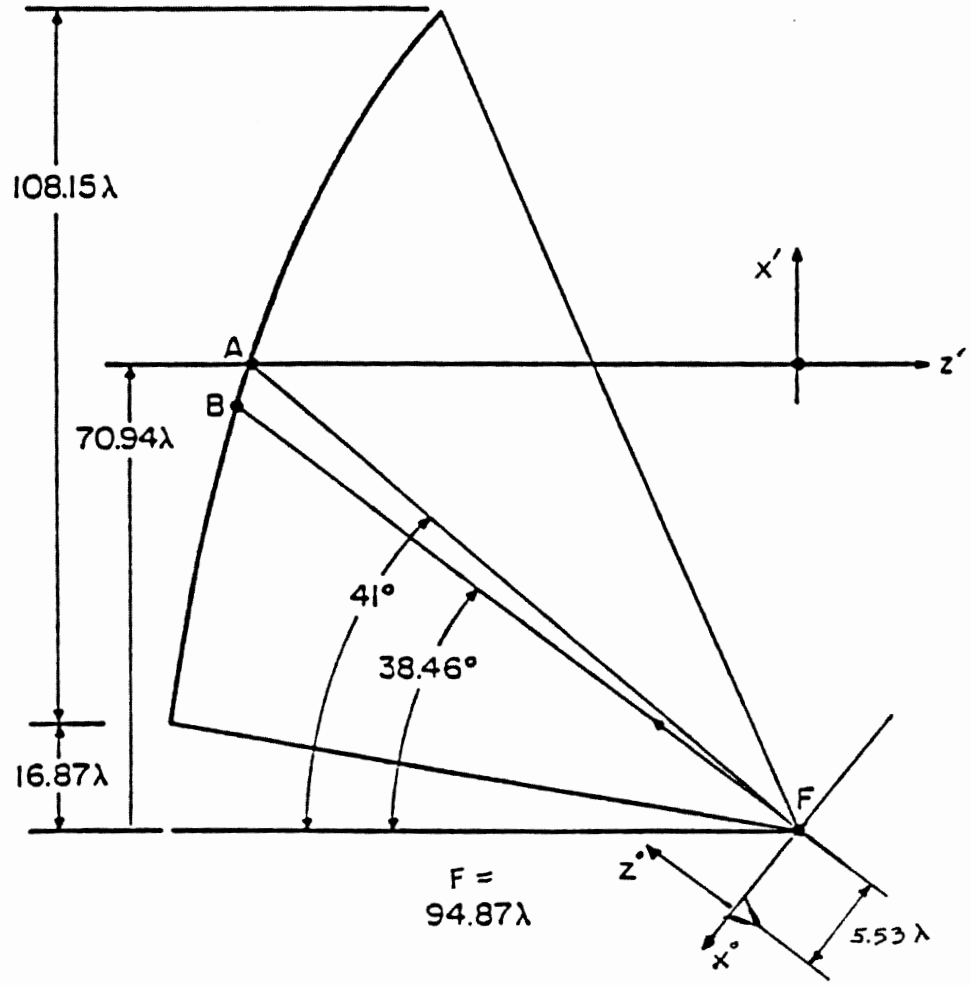


Figure 5.3.1-1 Reflector/Feed Array Geometry. From [19]

90, 180, 0.0, 180.0, 90.0

- Output:

Some specifics of the output are given below.

```
Maximum Reflector Gain   =  48.12 dB
Side lobe Level          = -13.5  dB (shoulder)
                           -24.05 dB (first lobe)
Cross Polarization Level = -46.77 dB
Aperture Efficiency      =  56.21%
Feed Gain                =  15.82 dB
```

Example 2

The same geometry of Figure 5.3.1-1 is used, however a 7 element feed cluster illuminates the reflector. This is a reproduction of P. T. Lam and Shung-Wu Lee [28] taken from the geometry of their paper [19]. The element spacing is 0.5λ and the element patterns are $q_E = 3.6$ and $q_H = 2.8$ to represent 1λ x 1λ square horns. The Conjugate Field Matched (CFM) weights are used below.

$$I_1 = 1.0 \angle 0.0^\circ$$
$$I_2 = I_5 = 0.783 \angle -8.0^\circ$$
$$I_3 = I_4 = 0.761 \angle 12.4^\circ$$
$$I_6 = I_7 = 0.821 \angle -3.9^\circ$$

Figure 5.3.1-1 shows the Reflector/Feed Array geometry.

- Input (LFN 20):

```
T, T, F, F, T, T, F, T, F, F

7, 0, 70

90.0, 141.54,   -90.0, -4.33,   0.0,   -3.44

0.0,    0.0,    0.0,    0.0,    0.0,    0.0

0.0,    0.0,    0.0,    0.0,    0.5,    0.0
```

```
0.0,    0.0,    0.0,   0.433,  0.25,   0.0
0.0,    0.0,    0.0,   0.433, -0.25,   0.0
0.0,    0.0,    0.0,    0.0,  -0.5,    0.0
0.0,    0.0,    0.0, -0.433,  -0.25,   0.0
0.0,    0.0,    0.0, -0.433,  0.25,    0.0
1.0,    0.0
0.783, -8.0
0.761, 12.4
0.761, 12.4
0.783, -8.0
0.821, -3.9
0.821, -3.9
3.6,    2.8
54,075, 54.075, 0.0, 0.0
94.87,  70.94
0
4,      20
1.0,    5.0,    0.05
0.0,    0.0,    90.0
90,     180,    0.0, 180.0,  90.0
```

• Output

The maximum reflector gain was calculated as 48.060 dB. The gain calculated by P. T. Lam and Shung-Wu Lee was 48.049 dB [28]. Excellent agreement is noted.

Example 3:

Example 2 is re-investigated with the automatic pointing option turned on. This option points the individual elements at the geometric dish center (point A) in Figure 5.2-2. The logical LPOINT is set T (True). and all elements are to be pointed (NPOINT = 7). The element weights are assumed equal, hence all given the excitation $1.0 \angle 0.0^{\circ}$.

• Output

The maximum reflector gain from this system is 48.04 dB. This is only 0.02 dB below that calculated by MFRAP in example 2. Conjugate field matching is hardly warranted due to the extra losses associated with the attenuators and phase shifters.

## 5.4 RESULTS AND COMPARISONS

MFRAP was tested in several ways. First, single elements were examined and compared with RAP outputs. The singlet geometry outputs compared very well. Then MFRAP was compared to outputs of different

methods. Table 5.4-1 gives a sample comparison [31]. Next multi-element geometries were tested.

Simple multi-element feed arrays were studied. Two and three isotropic elements forming broadside and endfire arrays were tested. Superposition of the far-field secondary patterns from each element were used for comparison purposes. MFRAP reproduced the far-field superposition without error in pattern and gain.

Table 5.4-1

GAIN AND SIDELOBE LEVELS OF OFFSET PARABOLIC REFLECTOR COMPUTED USING SEVERAL DIFFERENT METHODS*

| | Jacobi-Bessel | FFT | GTD | GO | Fourier-Bessel | MFRAP |
|---|---|---|---|---|---|---|
| Gain (dB) | 48.28 | 48.26 | 48.31 | 48.29 | 48.22 | 48.28 |
| 1st SL | 28.70 | 28.94 | 28.48 | 28.49 | 27.98 | 28.78 |
| 2nd SL | 22.50 | 22.64 | 22.64 | 22.78 | 21.92 | 22.53 |
| 3rd SL | 18.32 | 18.85 | 17.72 | 17.63 | 17.76 | 18.44 |
| 4th SL | 15.21 | 15.55 | 15.80 | 14.93 | 14.64 | 15.32 |
| 5th SL | 12.67 | 12.76 | 12.09 | 8.54 | 12.14 | 12.84 |
| 6th SL | 10.55 | 11.15 | 11.30 | 9.96 | 10.01 | 10.70 |

*From [31]

More complex geometries were studied next. Seven horn (high-directive) elements forming an array with a triangular lattice geometry was investigated. The geometry of Figures 5.3.1-1, 5.2-3 and 5.4-1 was used. The results of P. T. Lam and S. W. Lee were reproduced [28]. Note that Table III as published in [19] is incorrect. The correct magnitude and phase weights are given in Table 5.4-2 [28]. The directivity calculated by MFRAP and P.T. Lam are included. Excellent agreement is noted.

Table 5.4-2

Seven Element Cluster Comparison*

| Element Excitation Coefficients | Conjugate Field Matching | Optimum Directivity |
|---|---|---|
| $I_1$ | $1.000 \angle 0.0°$ | $1.0 \angle 0.0°$ |
| $I_2 = I_5$ | $0.783 \angle -8.0°$ | $1.347 \angle 123.6°$ |
| $I_3 = I_4$ | $0.761 \angle 12.4°$ | $1.229 \angle -161.0°$ |
| $I_6 = I_7$ | $0.821 \angle -3.9°$ | $1.175 \angle 176.0°$ |
| Gain | | |
| P. T. Lam ** | 48.05 dB | 48.61 dB |
| MFRAP | 48.06 dB | 48.62 dB |

*"High-Directive" Horns ($q_E = 3.6$, $q_H = 2.8$)

**Results obtained [28]

The same seven element cluster geometry was tested with low directive (dipole; $q_E = 1.0$ and $q_H = 0.0$) elements but with element spacings decreased to $0.4\lambda$. The weighting coefficients of P. T. Lam [28] were used and the results are compared to those of P. T. Lam in Table 5.4-3. Note that Table IV of [19] is incorrect. Results in Table 5.4-3 are in good agreement.

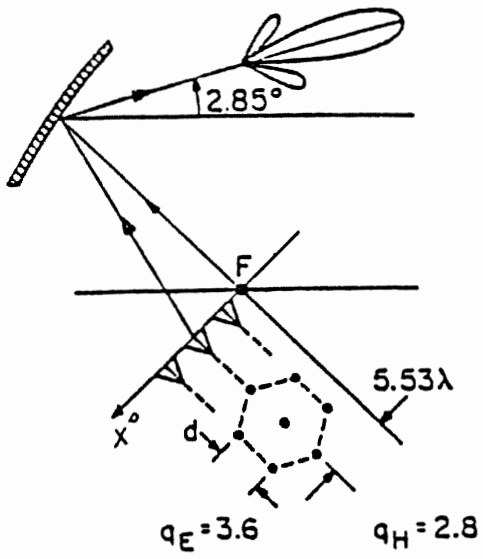


Figure 5.4-1. Seven element cluster (d = 0.5λ) illuminating offset reflector geometry. From [19]

Table 5.4-3

Seven Element Cluster Comparison*

| Element Excitation Coefficients | Conjugate Field Matching | Optimum Directivity |
|---|---|---|
| $I_1$ | $1.000 \angle 0.0°$ | $1.000 \angle 0.0°$ |
| $I_2 = I_5$ | $0.845 \angle -5.4°$ | $1.031 \angle 157.5°$ |
| $I_3 = I_4$ | $0.840 \angle 10.0°$ | $1.269 \angle -179.3°$ |
| $I_6 = I_7$ | $0.870 \angle -4.1°$ | $1.283 \angle 169.4°$ |
| Gain | | |
| P. T. Lam ** | 45.88 dB | 46.99 dB |
| MFRAP | 45.86 dB | 47.00 dB |

*" Low-Directive"Dipoles ($q_E = 1.0$, $q_H = 0.0$)

**Results obtained [28]

## 5.4.1 RESULTS OF ELEMENT POINTING STUDY

A short investigation was made on the effects of element pointing on reflector performance. The study gives a good representation of how MFRAP can be used to investigate multiple feed reflector configurations. The ability for MFRAP to analyze the reflector/feed array system as one step is important. Contrary to the secondary far-field pattern superposition approach, MFRAP has the ability to examine both feed array

and reflector performance in one step (code run). In all likelihood secondary pattern superposition requires at least two codes and many code runs. The outputs from these codes are used to determine the reflector/feed array performance. The one code run approach allows MFRAP to be combined with optimization methods where certain parameters can be optimized easily. In this study, an attempt was made to optimize reflector gain by repointing the feed elements(s).

It was speculated that reflector gain could be improved by simply repointing the feed elements toward the dish center. This concept was first studied using RAP [1]. The initial study showed that as reflector edge illumination became balanced minor improvements in reflector gain and side lobe level resulted. The study to be discussed extends the focused (non-scanned feed) results to scanned multiple feed systems.

The geometry of Figure 5.3.1-1 was used as the baseline reflector system. A single element projected dish (singlet) was placed at the focal point and pointed at points A (geometric center) and B (equal edge angle) of Figure 5.3.1-1. Table 5.4.1-1 shows the results from two separate horn representations. A typical horn used in in the cluster design ($q_E$ = 3.6, $q_H$ = 2.8) and a typical horn giving -10 dB edge taper ($q_E$ = $q_H$ = 9.0442) were investigated. The results show that repointed reflector systems react positively towards element re-pointing when high directive (-10 dB edge taper) horn type patterns are involved.

Table 5.4.1-1

Focused Singlet Pointing Results

| | "Cluster" Singlet ($q_E$=3.6, $q_H$=2.8) | | -10 dB Edge Taper Singlet ($q_E$=$q_H$=9.0442) | |
|---|---|---|---|---|
| Singlet Pointed at* | A | B | A | B |
| Maximum Reflector Gain (εap) | 48.28 dB (58.31)% | 48.29 dB (58.36)% | 49.69 dB (80.56)% | 49.67 dB (80.23)% |
| Sidelobe Level (dB down) | -19.55 | -19.63 | -24.63 | -24.00 |
| Cross-Pol (dB down) | -23.66 | -24.67 | -24.79 | -25.35 |

*See Figure 5.2-2 for pointings.

Repointing the lower directive (-3 dB edge taper) elements produced little change. This is expected because higher directive elements (high q) have sharper patterns increasing sensitivity to pointing.

The examination of the effects of element pointing was extended to cluster feed designs. The singlet was replaced with a seven element cluster of Figure 5.2-3 with d = 0.5λ. Equal magnitude and phase weights ($1.0 \angle 0.0°$) were used throughout. Two cluster pointing geometries were studied. First, a planar array with all elements pointing in the same direction were used. The central element was pointed toward point B. The surrounding elements were aligned (not rotated, only translated) with

the central element. The Eulerian angles for the surrounding elements were therefore zero. In a seond set of calculations each element of the planar array was pointed toward point A. The results from the two different pointing geometries are given in Table 5.4.1-2. Improvement is noted for the second case. Note that the cross-polarization level increased for the individually pointed elements. This is due to the small misalignments inherently generated when the elements are unequally pointed.

Table 5.4.1-2

Focused Cluster Pointing Results

| | Equal Pointing (Central Element pointed at B) | Unequal Pointing (elements individually pointed at A) |
|---|---|---|
| Maximum Reflector Gain ($\varepsilon_{ap}$ %) | 49.58 dB (78.71%) | 49.59 dB (78.89%) |
| Side Lobe Level (dB down) | -23.05 | -23.16 |
| Cross-Polarization Level (dB down) | -25.18 | -25.25 |

*elements were $\cos^{q}\theta$ with $q_E$=3.6 and $q_H$=2.8

Scanned singlet geometries were studied next. Figure 5.4.1-1 shows the pointing used for the five and ten beamwidth scans. The translation vector for the 5 BW scan was $\bar{w}_c^o$ = -4.33 $\hat{x}$ + 0.0 $\hat{y}$ - 3.44 $\hat{z}$ (in

wavelengths). The ten beamwidth translation vector was $\bar{w}_c^o = -8.34\ \hat{x} + 0.0\ \hat{y} - 6.63\ \hat{z}$. Table 5.4.1-2 gives the results for each scan. The results indicate that element pointing has more effect on reflector performance as the feed is moved away from the focal point. It is interesting to note that "pointing #2" produces less gain than "pointing #1" for the ten BW case. Scan loss is related to the unequal phase illumination (phase tilt) created by the scanned elements. Re-pointing the element controls magnitude illumination only. Therefore scan performance is best improved with phase control which removes (or lessens) the phase tilt. Cluster feed designs allow phase control because the individual elements can be phase weighted. The scanned cluster is examined next.

## Table 5.4.1-3

Scanned Singlet Pointing Results

Singlet ($q_E = q_H = 9.0442$).

| | Pointing* #1 | Pointing* #2 |
|---|---|---|
| 5BW scan Maximum Reflector Gain (εap%) | 48.12 dB (56.21) | 48.21 dB (57.42) |
| 10 BW scan Maximum Reflector Gain (εap%) | 44.58 dB (24.89) | 44.29 dB (23.38) |

*See Figure 5.4.1-1 for pointings

Scanned seven element cluster designs were examined. The elements were equally weighted. Figure 5.4.1-2 shows the pointings used. Table 5.4.1-2 gives the results. As expected, the results are consistent with the scanned singlet geometries. Phase control must be employed to increase performance of scanned reflector systems [30]. This phase control can be accomplished by phase weighting the individual elements.

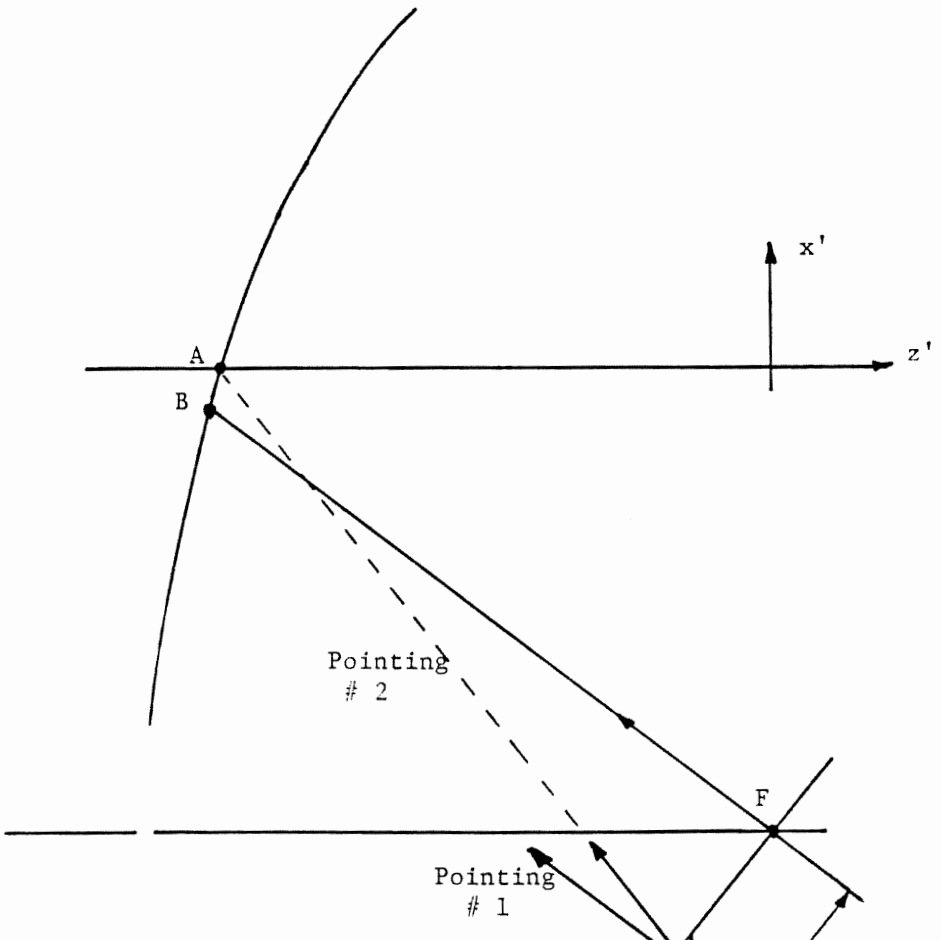


| s | BW |
|---|---|
| 5.53λ | 5 |
| 10.65λ | 10 |

Figure 5.4.1-1 Singlet pointing angle geometries.

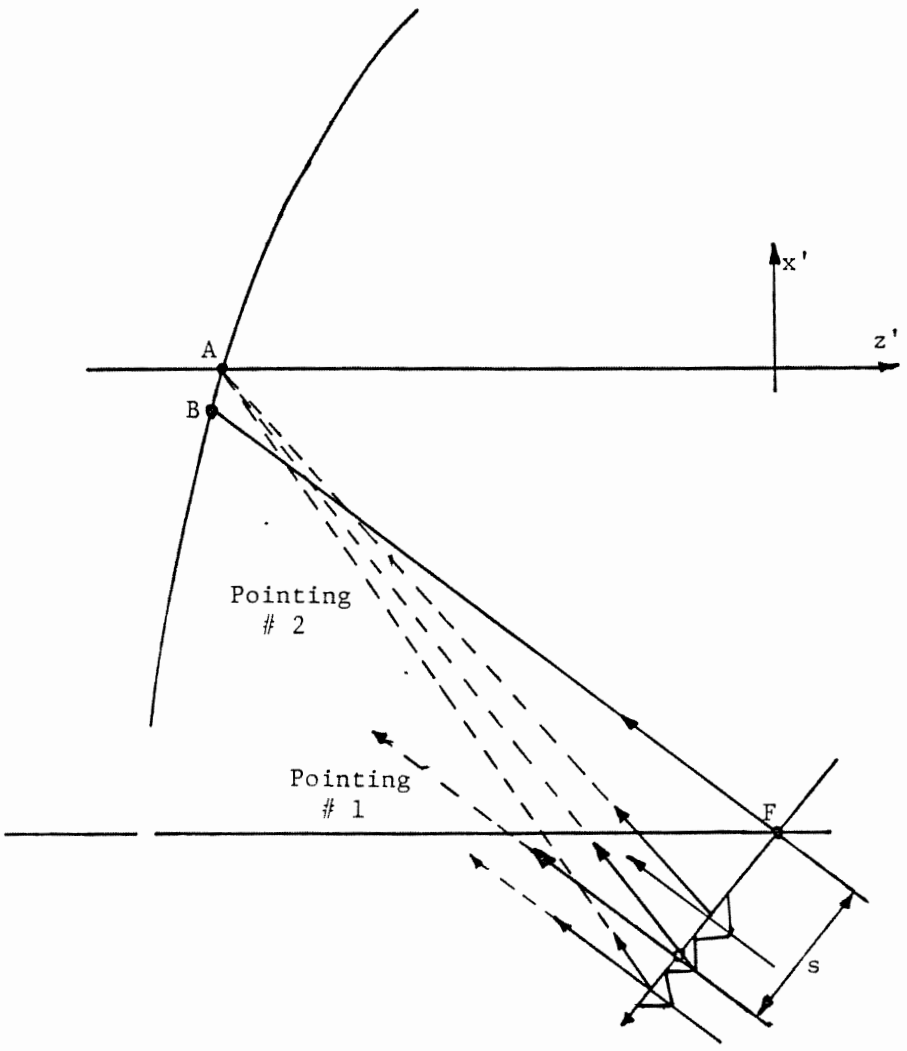


Figure 5.4.1-2 Scanned seven element cluster pointing geometries.

## Table 5.4.1-4

Scanned Cluster Pointing Results

| | Peak Reflector Gain ($\varepsilon_{ap}$%) | |
|---|---|---|
| | Pointing #1 | Pointing #2 |
| 5 BW scan | 47.96 dB (54.19) | 48.04 dB (55.21) |
| 10 BW scan | 44.15 dB (22.52) | 43.88 dB (21.16) |

# 6. CONCLUSIONS

A method of calculating the secondary pattern of a reflector antenna illuminated by a feed array was developed and programmed. Physical optics was used to form the radiation integral which was evaluated using a back-to-back Gaussian-Legendre quadrature. Geometrical optics was used to find the incident field from each feed element at the reflector surface. These fields were superimposed to form the total incident field used in calculating the surface currents of the radiation integral.

The feed element field superposition method has been proven accurate, efficient and useful. Theory allows for (each element) arbitrary position, orientation, excitation (magnitude and phase) and pattern. The advantages are:

(i) Accurate feed array spillover values can be obtained leading to accurate gain and efficiency values.

(ii) The multi-element feed can be analyzed almost as fast as a single element and requires far less file management.

(iii) The elements can be arbitrarily located and pointed which is ideal for feed location and pointing optimization studies.

## 7.0 REFERENCES


1. W. L. Stutzman, S. H. Stewart, T. Pratt "Innovative Design of Satellite Earth Terminal Antennas", Final Report, Report No. SATCOM T85-4, VPI & SU Project 230-11-110F-104-8026631, Nov. 1985.

2. M. Safak, "Forward Radiation from axially symmetric reflector antennas," IEEE Trans. on Ant. and Prop., vol. AP-32, pp 893-901, September 1984.

3. F. J. V. Hasselmann and L. B. Felsen, "Asymptotic analysis of parabolic reflector antennas," IEEE Trans. on Ant. and Prop., vol AP-30, pp 677-685, July 1982.

4. G. L. James and V. Kerdemelidis, "Reflector antenna radiation pattern analysis by equivalent edge currents," IEEE Trans. on Ant. and Prop., vol. AP-21, pp. 19-24, January 1973.

5. P-S Kildal, "On the accuracy of physical optics," IEEE Trans. on Ant. and Prop., vol, AP-30, pp. 9-12, May 1982.

6. W. V. T. Rusch and P.D. Potter, Analysis of Reflector Antennas, Academic Press: New York, 1970.

7. A. W. Rudge, "In Defense of Aperture-Field Theory, "U. of Birmingham Electronic and Electrical Eng. Dept. Memorandum No. 441, Nov. 1972.

8. A. W. Rudge and M. Shirazi, "Multiple Beam Antennas: Offset Reflectors with Offset Feeds," U. of Birmingham Electronic and Electrical Eng. Dept. Final Report to ERSO/ESTEC under Contract No. 1725/72 PP, 25 July 1973.

9. Yahya Rahmat-Samii, "A comparison between GO/aperture-field and physical optics methods for offset reflectors," IEEE Trans. on Ant. and Prop., vol. AP-32, pp. 301-306, March 1984.

10. A. W. Rudge, "Multiple-beam antennas: Offset reflectors with offset feeds," IEEE Trans. on Ant. and Prop., vol. AP-23, pp. 317-322, May 1975.

11. N. A. Adatia, Cross-Polarization of Microwave Reflector Antennas," PH.D. Thesis, Univ. Survey, England, 1974.

12. S. W. Lee, et al., "Diffraction by an Arbitrary Subreflector: GTD Solution," IEEE Trans. on Ant. and Prop., vol. AP-27, no. 3, May 1979, pp. 305-316.

13. W. T. Rusch, "A Comparison of Geometrical and Integral Fields from High-Frequency Reflectors," Proceedings of the IEEE, Nov. 1974, p. 1603.

14. Y. Rahmat-Samii, "Shaped reflector antenna analysis using the Jacobi-Bessel series," IEEE Trans. on Ant. and Prop., vol. AP-28, pp. 425-435, July 1980.

15. V. Galindo-Israel and R. Mittra, "A new series representation for the radiation integral with application to reflector antennas," IEEE Trans. on Ant. and Prop., vol. AP-25, pp. 631-641, September 1977.

16. R. Mittra, et al., "An efficient technique for the computation of vector secondary patterns of offset paraboloid reflectors," IEEE Trans. on Ant. and Prop., vol. AP-27, pp. 294-304, May 1979.

17. Y. Rahmat-Samii, "Useful coordinate transformations for antenna applications," IEEE Trans.on Ant. and Prop., vol. AP-27, pp. 571-574, July 1979.

18. W. L. Stutzman and G. A Thiele, Antenna Theory and Design, John Wiley: New York, 1981.

19. P. T. Lam, S. W. Lee, D. C. D. Chang, and K. C. Lang, "Directivity Optimization of a Reflector Antenna with Cluster Feeds: A Closed-Form Solution," IEEE Trans. on Ant. and Prop., vol. AP-33, Nov. 1985.

20. S. W. Lee, Y. Rahmat-Samii, "Simple Formulas for Designing an Offset Multibeam Parabolic Reflector," IEEE Trans. on Ant. and Prop., vol. AP-29, May 1981.

21. A. C. Ludwig, "The definition of cross polarization," IEEE Trans. on Ant. and Prop., vol, AP-21, pp. 116-119, January 1973.

22. W. L. Stutzman, "Mathematical Formulations and Definitions for Dual Polarized Reception of a Wave Passing Through a Depolarizing Medium (A Polarized Primer)," Virginia Tech Satellite Communications Group Technical Report No. 77-4, 1977.

23. L. W. Johnson and R. D. Riess, Numerical Analysis, sec. edition, pp. 301-302, 1982.

24. P-S. Kildal, "Factorization of the feed efficiency of paroboloids and cassegrain antennas," IEEE Trans. on Ant. and Prop., vol. AP-33, pp. 903-908, August 1985.

25. Phone conversations with D. E. Ball and M. D. Vanstrum, March and May 1986.

26. P. Clarricoats, S. Tun, and R. Brown, "Performance of offset reflector antennas with array feeds," IEEE Proceedings, vol. 131, no. 3, June 1984.

27. Y. Rahmat-Samii and S. W. Lee, "Directivity of planar array feeds for satellite reflector applications," IEEE Trans. on Ant. and Prop., vol. AP-31, pp. 463-470, 1983.

28. Phone conversation with Dr. Shung-Wu Lee on May 16, 1986.

29. H. E. King and J. L. Wong, "Directivity of uniformly excited N x N array of directive elements", IEEE Trans. on Ant. and Prop., vol. AP-23, no. 3, pp. 401-404, May 1975.

30. V. G. Israel, S. W. Lee and R. Mitra, "Synthesis of a laterally displaced cluster feed for a reflector antenna with application to multiple beams and contoured patterns," IEEE Trans. on Ant. and Prop., vol. AP-26, no. 2, pp. 220-228, March 1978.

31. P. T. Lam, et al., "Strategy for reflector pattern calculation: Let the computer do the work," IEEE Trans. on Ant. and Prop., vol. AP-34, no. 4, April 1986.

The vita has been removed from the scanned document